Improving the Robustness of Urban Electricity Networks
IRENE

D3.1 System architecture design, supply demand model and simulation

Document version:	**2**
Document status:	Final
Project Document Date:	31.03.2016
Contributing Workpackage:	WP3
Dissemination level:	P

Author(s):
Sandford Bessler, Oliver Jung (AIT),
Eng Tseng Lau, Kok Keong Chai, Yue Chen (Queen Mary University of London)
Alexandr Vasenev (University of Twente)
Andrea Ceccarelli, Andrea Bondavalli (University of Florence)
Tony Clarke (Ethos)

Table of Contents

1 EXECUTIVE SUMMARY

The purpose of this deliverable that is related to WP3 (System Architecture, Methodologies and Policies) of the Project IRENE, is to describe the planning approach and the architecture of the tools for improving the resilience of an urban power grid.
The response of the power grid as a result to an outage is often a complete blackout, sometimes the grid contains islands of operating grids, and – this is the novelty in our approach- in some cases the grid can operation with a reduced demand. The outcome depends of the of the outage scenario: did one of the N power generators fail (N-1 contingency)? Did an important power line clip disconnecting several substations? Did a substation or transformer fail or did the grid mains fail?
In this Deliverable we develop models for the characterization of consumption data, as well as the architectural basis to develop tools for the evaluation the effect of outages in different levels of the grid. In a mid-voltage, urban distribution grid, we handle outages that lead to topology changes, individual link and node (generation) failures, etc., whereas at the microgrid level, we do not handle individual node or link failures, but use flexible loads and demand management mechanisms for a "soft" degradation of service (see also Section 2.2).

In Chapter 3 of the deliverable, a meshed distribution grid is considered. The model of the grid is quite generic and is not restricted to a certain e.g. radial topology, to a certain voltage level or to a certain limitation of node power consumption.
The contributions of this chapter refer to the preparation of consumption data, energy balancing and optimization mechanisms and failure handling as detailed below:

- A method for predicting the electric consumption of different buildings using the day-night, week-weekend and seasonal periodicity and an aggregation technique using the Ensemble Kalman Filter. Different types of building profiles are created.
- An energy balancing optimization based on a cost minimization function is presented and is combined with the determination of economic balancing the output of generation units (unit commitment).
- The modelling and effects of storage units (batteries) is evaluated in normal case
- Scenarios for a grid outage operation concentrate on the N-1 contingency (failure of one generation unit), or complete islanding, but mention the economic caused islanding as well.
- Resiliency in energy grids as defined in previous work is reviewed.

In Chapter 4 of the deliverable, at the microgrid level, direct load control at the level of microgrid and at the lower level of a building is performed. This can work without user comfort reduction only if load flexibility is used (such as in heating, cooling, use of batteries or electric cars).

- A concrete microgrid control architecture that will be used for the simulation of normal operation and outage events. Microgrid and building controller mathematical optimization models have the purpose to provide demand management functionality.
- Resiliency is reformulated in form of an autonomy factor in order to cope with the effect of demand side management.
- Test results are described that underline the autonomy factor dependency of renewable generation, outage duration and dispatchable generation capability.

The models applied to different levels of the grid will be used in the development of planning tools in WP4.

1.1 GLOSSARY

CB	Circuit breaker
EnKF	Ensemble Kalman Filter
ESS	Electric Storage System
EV	Electric Vehicle
HVAC	Heating Ventilation Air Conditioning
SOC	State of charge
RES	Renewable sources
CEMS	Customer Energy Management System
MPC	Model predictive control
DG	Distributed Generator

2 INTRODUCTION

2.1 ISLANDING: NEEDED FEATURES AND THE PROCESS

This subsection illustrates recent examples how distributed generation (DG) can support critical infrastructures and what features should be considered to make it possible. Herewith we list the requirements to a microgrid as (1) four features to ensure uninterrupted operation during a utility system outage and (2) two steps needed to perform controlled islanding.

The amount of installed DG and the corresponding operational experience allows to say that their utilization during blackouts is common practice. According to a US DoE study[1], in 2007 about 12 million DG, including photovoltaic solar arrays, micro-turbines, and fuel cells, as well as CHPs, were installed in the US with a total capacity of about 200 GW. Most of these were back-up units used by customers to provide emergency power during times when grid-connected power is not available.

In the future, with further advances in distribution generation that feed the distribution grid, rather than the bulk transmission grid, these solutions can support grid clients both in time of (1) normal operation and in (2) crisis scenarios. In the first case, DG provide opportunities for electric utilities to reduce peak loads, as well as improve power quality. At the same time, DG can also be used to decrease the vulnerability of the electric system to threats from terrorist attacks and other forms of potentially catastrophic disruptions.

A number of examples how local power generation can assist in supporting critical infrastructures during time of blackout is provided in literature. For instance, a report[2] about more than ten case studies suggests that "Combined heat and power (CHP) offers the opportunity to improve CI resiliency, mitigating the impacts of an emergency by keeping critical facilities running without any interruption in electric or thermal service." The report lists four features needed to ensure uninterrupted operation during a utility system outage:

1. Black start capability (the need for a battery powered starting device or other supplemental electricity supply system, such as a backup generator, that will allow it to start up independently from the grid);
2. Generation capable to continue operation without the grid power signal (e.g. synchronous generators and supporting controls).
3. Ample carrying capacity;
4. Parallel utility interconnection and switchgear control. This includes the need for the system to reconnect itself smoothly after an event.

[1] "The potential benefits of distributed generation and rate-related issues that may impede their expansion" http://www.ferc.gov/legal/fed-sta/exp-study.pdf, p. iii

[2] "Combined Heat and Power: Enabling Resilient Energy Infrastructure for Critical Facilities", http://www1.eere.energy.gov/manufacturing/distributedenergy/pdfs/chp_critical_facilities.pdf, 2013

The need for elements can be identified in the case of CHP operating at Greenwich Hospital, Connecticut, USA. In 2012 its CHP consisted of two 1.250 kW natural gas-fired reciprocating engines next to 2.000 kW backup generator. This capacity was sufficient to carry critical loads (feature 3) and even disconnect the hospital off the grid, if a demand response program demands that. After the hospital lost power, it went down for about 7 seconds before the backup generators kicked in. The whole transition to CHP system takes approximately 5 minutes. This reflects the first feature. With the area around lost power for approximately 7 days, the hospital admitted 20 additional patients during the outage period.

The Sendai microgrid[3] can serve as another example how a microgrid can support critical infrastructures and prevent casualties. In this case, a grid located at Tohoku Fukushi University in Sendai City, Japan operated during 3 days in the aftermath of the Tohoku Earthquake in 2011. The grid, composed of two gas engines (2x350 kW), a phosphoric acid fuel cell (PAFC 200kW), and a photovoltaic array (50 kW), was designed to support different classes of electricity consumers. The classes were, including a DC Power class that required uninterrupted power supply. Two aspects are particularly noteworthy in connection to this accident. First, the grid allowed to supply energy to a class of load that initially was not within the island perimeter: the nursing care facility with four elderly people, dependent on ventilators for life support. In this way, it supported feature 3 of the above list. At the same time, the microgrid had a difficulty to start gas engines, because the control system batteries were totally discharged, and did not recover until about a day later. This aspect, related to Black start capability, was therefore not in line with the first feature outlined above and hampered the microgrid utilization during the blackout.

In addition to considering these four features, mainly related to physical components of a microgrid, the system also need to be capable to perform steps to form islands at pre-selected locations. In case of Controlled islanding[4], the procedure need to account for two steps: (1) create a balance between the load and generation before the isolation from the system (including changing the topology) and (2) to isolate the island from the system. Both the cyber components and physical components of microgrids are involved in this process. If these cyber-physical assets are physically destroyed (e.g. due to an earthquake), temporary out (tripped), or operate at a degraded capability (for instance, a DDoS attack resulted in communication delays), the islanding may fail.

While operating during a prolonged outage a microgrid might account for failures within the microgrid itself. Therefore, a microgrid can benefit by adapting its topology. High Reliability Distribution System (HRDS) introduced by Illinois Institute of Technology[5] illustrates this idea. This microgrid includes several loops. Each building is connected to a loop using switches. In case of a faulted cable it allows to directly isolate it and avoid disconnecting all other connected loads. It is automatic switches in HRDS that can sense the cable faults and isolate the faulted section with no impact on other sections in a microgrid. Master controller,

[3] The Sendai Microgrid Operational Experience in the Aftermath of the Tohoku Earthquake: A Case Study

[4] http://smartgrid.epri.com/UseCases/ControlledIslanding.pdf

[5] http://www.iitmicrogrid.net/microgrid/index_all.htm

in turn, monitors the status of each HRDS switch using the supervisory control and data acquisition (SCADA) system, and is responsible for economic operation of the microgrid.

Altogether, for establishing and operating as an island the microgrid should possess a set of features and be capable to island securely by following the two-step procedure. The features and the functions within the procedure can be seen as a checklist to ensure that the islanding can be successful.

2.2 THE APPROACH

The project IRENE intends to develop a collaborative set of tools for city planners to analyse an urban grid and create a so called heat map with respect to its vulnerability against power outages, trying to answer following questions:

- which power generating grid nodes are more vulnerable to outages and what is the effect of their failure to the rest of the grid
- which nodes have enough local generation capacity to be self-sufficient
- what demand level require the rest of the nodes during an outage, given that demand side management, RES and ESS are used.

According to the description of work, this deliverable is a result of WP3, which develops mitigation measures for the threats in WP2. The measures include the planning of islanding capabilities, installed DER and energy storage capacity, reduced supply through demand flexibility options, load prediction and needed ICT communication infrastructure & controllers and security mechanisms.

Although an outage event may affect the national grid and via the transmissions system - an entire continent, we think that the mitigation mechanisms have to be detailed, limited in scope.
The approach has been to divide the studied grid - an urban distribution grid which can consist of hundreds secondary substations (low voltage grids) – into a high and a low level. The main reason for that is the different methods that can applied at each of the levels:

The higher level is a mid voltage grid of the region in consideration in which the failing components are power plants, lines, stations (SCADA), current breakers, etc. Following an outage contingency, schemes are applied a) to isolate grid portions and drop load or b) to connect alternatively a grid region, which has been disconnected from their main supply. Chapter 3 will discuss this level: data preparation (prediction), energy optimization models, balancing the output of power plants (unit commitment problem) and redistribution of energy in case of failure of a generating node (N-1 contingency).

The second level is the low voltage grid, where the topology is mostly radial and consists of several feeders. The model described in Chapter 4 is more detailed going down to buildings, and individual loads and generators. We choose self organizing structures, called microgrids in which renewable sources (RES) and flexible loads play a major role. Due to their flexibility, reliability and islanding capability, microgrid architectures are proposed in the literature (Lopes 2009), (Katiraei 2005). The overall energy control mechanism used in the microgrid is demand management. Two outage scenarios are discussed: in the first one, an external outage event triggers an emergency mode which causes the reduction of the consumption in the microgrid. In the second scenario, the microgrid is islanded and has to use local dispatchable generation to balance the (reduced) consumption.

The proposed integration of the two levels is shown in the Figure: a certain outage scenario is simulated. In order to obtain the behaviour of individual LV grid (microgrids) the computation is delegated to the microgrid level. The collected results allow to compute the overall load distribution for the configured outage situation. Alternatively, one can plan for self sufficient microgrids which would go in islanding mode in case of an external outage. In this case a different power flow distribution will be computed.

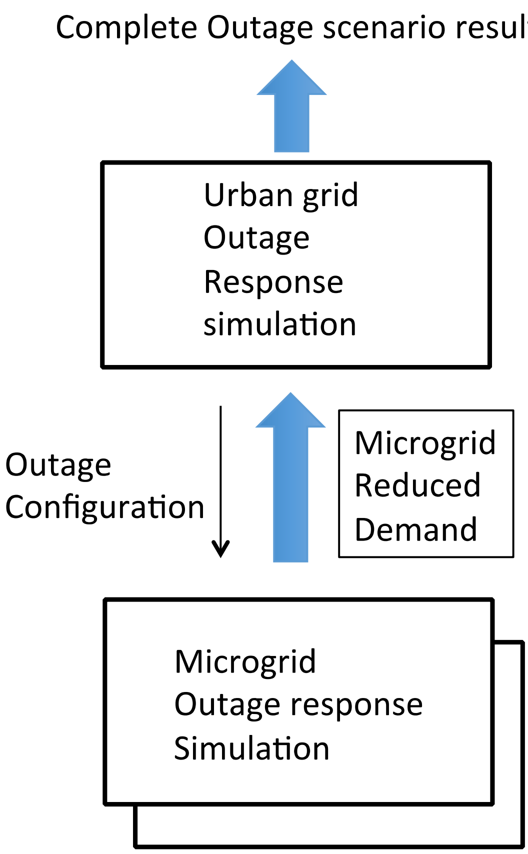

3 Mid Level Grid Model

3.1 Introduction

The grid model in this section should cover the scope envisaged in the IRENE project, namely an urban grid, therefore it can cover both mid voltage grid elements such as stations, substations, DER, power plants, power lines.

The model will be integrated in an operation costs optimisation formulation in Section 3.4, subject to operational constraints and contingency criteria.

The first grid example in Figure 3-1 shows a microgrid, whereas the example in Figure 3-2 is a general grid (14 bus IEEE Test grid). These very different networks underline the generic character of the high level IRENE grid model.

The contributions in this Chapter can be structured as follows:

- methods for creating demand data at different aggregation levels (profiling), and simulation results (Sections 3.6.1, 3.6.2)
- computation of operation costs, including generation costs of local power plants, and energy costs from the main grid, battery storage costs , etc.
- optimization simulation results for three scenarios (normal operation, failure of one power plant, islanded grid), Section 3.6.3.

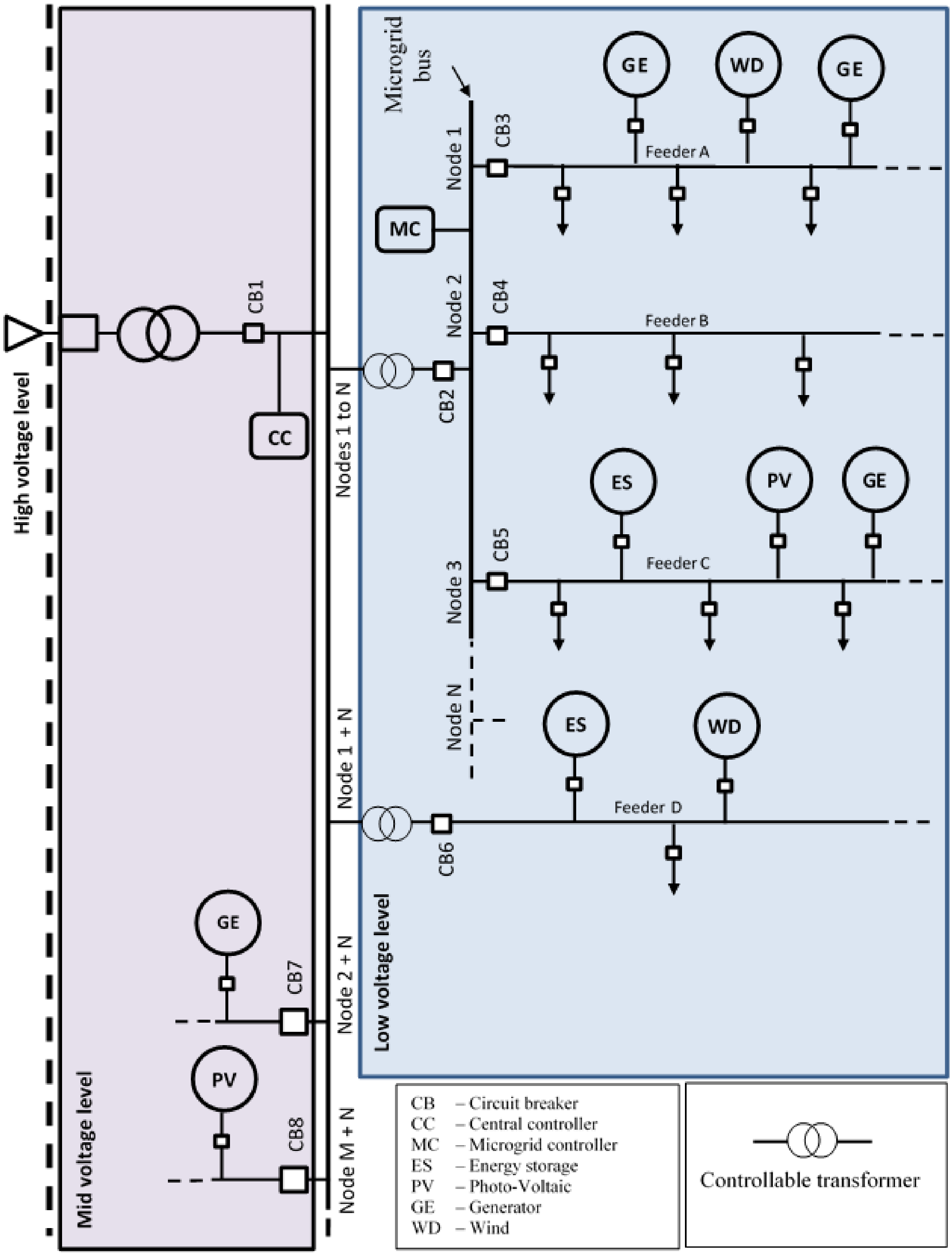

Figure 3-1: **A microgrid configuration. Adapted and modified from (Huang & Zhuang, 2014; NACHHALTIGwirtschaften, n.d.).**

Based on Figure 3-1, each node (Node 1, Node 2, …, Node M+ N) consists of the component of mid and low voltage distribution network that includes the generators (in the mid-voltage level) and electrical loads for the end consumers and small scale distributed generators that are connected via electrical interconnectors for the low-voltage level. Both *M* and *N* denote the number of nodes for the mid-voltage level and low voltage level correspondingly. Distributed generators in the microgrid are typically represented as the distribution substations (the collection and distribution of power for the grid) that are connected to feeders (Huang & Zhuang, 2014). The feeders will transfer the power from distributed generators from the distributed substation to the distribution transformers for the end consumers (Huang & Zhuang, 2014). The microgrid is connected to the mid-voltage grid through the transmission line. A circuit breaker, CB1, is installed that acts as the protection mechanism to connect or disconnect the mid-level grid from the high level grid. Similarly, CB2 is used to protect the microgrid (low level) from the mid-level grid.

A grid can have two operation modes: normal (grid-connected mode) and isolate grid portions (islanded mode). In the normal state, the microgrid is interacted with the mid-level grid. On the contrary, during an emergency event (contingency state), the microgrid can operate in an islanded mode by opening CB1 or CB2. This is to enable the continuous supply of power within the microgrid without interruptions, especially to the critical loads. The distributed generators will be activated to provide the power to the microgrid. Similarly, the mid-level grid can still operate by transferring power to the low level grid by opening CB1. In addition, an islanded operation can also occur within microgrid nodes. For example, all the components in Node 1 of the microgrid can be operated in islanded mode if CB3 is opened. The remaining nodes are still able to interact with the mid-level grid in the normal mode of operation.

A standard multi-bus system describing the interaction within the low voltage (microgrid) and the mid-level voltage is needed. To this end, A IEEE 14-bus system will be used. An example of the one-line diagram IEEE 14-bus system describing the interconnected grid is shown in Figure 3-2.

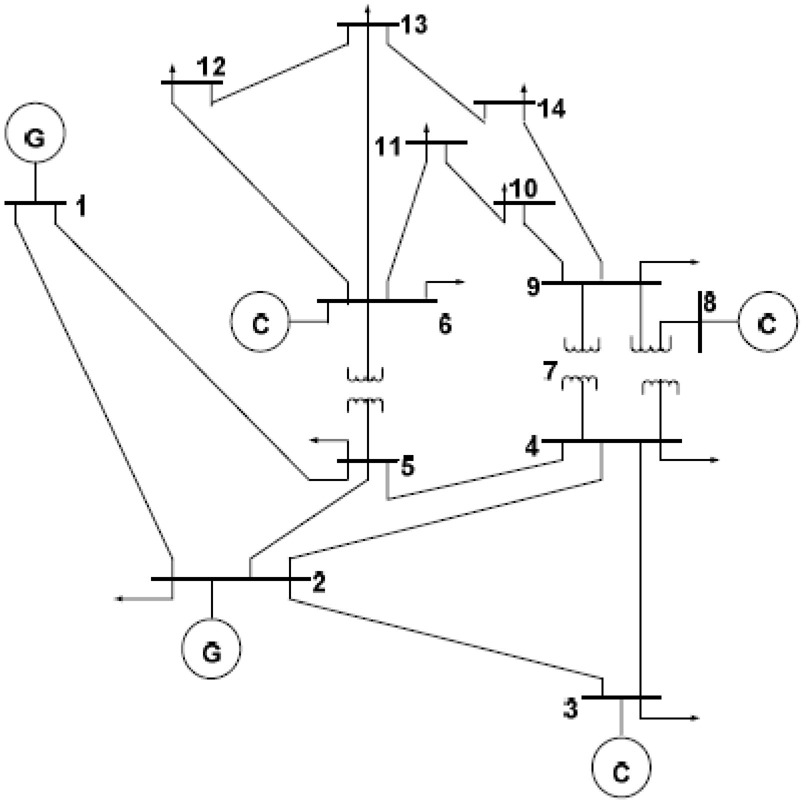

Figure 3-2: A one-line diagram of IEEE 14-bus system. Source: (Dike & Mahajan, 2008).

From the example in Figure 3-2, the author (Dike & Mahajan, 2008) considered two generators in buses One and Two, voltage sources in buses Three, Six and Eight, a transformer bus in bus Seven without load and voltage source, and the remaining buses with electrical loads. Notably, the buses can be represented as the nodes, and loads are further denoted as the end-consumer loads (low voltage level), and the voltage sources are the transmitted voltage from the mid-level grid. Additionally, the mid-scale generating units for the mid-level grid or the distributed generators in the low level grid can be considered in any of the buses. As there are numerous configurations associated to the 14-bus system (due to different scenarios considered), therefore the configuration and architecture of the grid in this case is not limited to the grid architecture as outlined by (Dike & Mahajan, 2008). In this case, the nodes and components outlining the topology of the grid will be defined. Such network topology will demonstrate the capability and flexibility of the grid operation either in the normal or islanding operations.

In this section, the in-depth grid operations are discussed, where the section begins with the demand profiling of lower-voltage network that later will contribute to overall demand across the mid-voltage level, the demand forecast and assimilation, the modeling of the optimisation tool, results and summary.

3.2 Demand Profiling

3.2.1 Notation

Indexes:

g	Generating units
i	Generating units during the islanding operation
n	Types of input profiles and components
k	Model state variable
j	Ensemble member index
r	Renewable generating units
s	energy storage
t	Time step index

Parameters:

Δt	Time interval in the storage operation
ε	Signal noises
C_t	Electricity market price at the time t
DT_g	Minimum down time of a generating unit g
I_{gt}	Binary values of commitment state of unit g
N	Total number of profiles
N_e	Total number of ensemble member
NG	Total number of generators
NG'	Total number of generators during the islanding operation
NR	Total number of renewable generations
NR'	Total number of renewable generations during the islanding operation
NS	Total number of storage
NS'	Total number of storage during the islanding operation
NT	Total number of time step
MO	Total number of must-off constraint
MR	Total number of must-run constraint
$P_{G,g}^{\min}$	Minimum allowable capacity of generator g
$P_{G,g}^{\max}$	Maximum allowable capacity of generator g
SU_g	Start-up cost of generators g
SD_g	Shutdown cost of generators g
T_1	Annual periodicity
T_2	Diurnal periodicity
UR_g	Ramp up rate at generator g
UT_g	Minimum up time of a generating unit g
DR_g	Ramp down rate at generator g

Variables:

$\alpha_{\text{Resiliency}}$	Resiliency index
d	Actual measurement (the model prediction)
$d_{obs,j}$	Ensemble of perturbed observations at jth ensemble member
m	Model parameters of the energy consumption profile
u_{gt}	Start-up variable at generator g at time t
v_j	Measurement noise at jth ensemble member
w_{gt}	Shut-down variable at generator g at time t
w_j	Model process noise at jth ensemble member
x_{gt-1}	Number of hours of the generating unit g has been switched on (+) or off (-)

y^{p}	Priori state vector y
y_{j}^{p}	Priori ensemble at jth ensemble member
y_{j}^{u}	Posteriori ensemble at jth ensemble member
$A\left(\frac{t}{T_1}\right)$	Annual cycle function
$D_k\left(\frac{t}{T_2}\right)$	Diurnal cycle function
$F_g(P_{G,gt})$	Generation cost function of generator g at time t
$N1_{G,it}^{c}$	Binary parameter for N-1 contingency state of the generating unit i at time t
$N1_{M,t}^{c}$	Binary parameter for N-1 contingency state of the transmission line between the microgrid and the main grid
$N1_{S,it}^{c}$	Binary parameter for N-1 contingency state of the energy storage unit i at time t
$P_{D,t}$	Total aggregated power across the grid at time t
$P_{D,t}^{c}$	Total aggregated power across the grid at time t during the contingency (islanding) operation
$P_{D,t}^{c'}$	Fraction of the demand served during the contingency (islanding) operation
$P_{G,gt}$	Power generated by corresponding generating unit g at time t
$P_{G,it}^{c}$	Power generated by corresponding generating unit i at time t during the contingency (islanding) operation
$P_{M,t}$	Power of the transmission line at time t
$P_{M,t}^{c}$	Power of the transmission line at time t during the contingency (islanding) operation
$P_{R,rt}$	Renewable power generated at renewable generators r at time t
$P_{R,it}^{c}$	Renewable power generated at renewable generators i at time t during the contingency (islanding) operation
$P_{S,st}$	Power generated in the energy storage s at time t
$P_{S,it}^{c}$	Power generated in the energy storage i at time t during the contingency (islanding) operation
$P_{SOC,it}^{c}$	SOC of the energy storage i during the contingency (islanding) operation
$P_{SOC,st}$	SOC of the energy storage s
$P_{SOC,i}^{\max}$	Maximum allowable SOC of energy storage i during the contingency (islanding) operation
$P_{SOC,i}^{\max}$	Maximum allowable SOC of energy storage s
R_t	Amount of reserve requirement at time t
RMSE	Root mean square error
$X_n(t)$	True state of electrical consumption for nth component at time t
Y^{p}	Collection of individual priori ensemble member y_{j}^{p}

3.2.1 Related background – state of the art

The demand profiling concept is established after the inception of the 1950's Electricity Council Load Research and followed by the 1998 Electricity Pool Programme (Elexon, 2013).

Such concepts are established to collect, analyse and develop the detailed knowledge of the consumption habits, either in domestic or non-domestic usage (Elexon, 2013; DoE, 2011). The demand profiling of the low voltage networks is strictly essential in providing the aggregated demands across the mid voltage level grid of a region. The electricity grid operator nowadays uses demand profiling as the important strategy to plan the amount of electricity to be provided to the entire network. Additionally, demand profiling also illustrates the present, upcoming and future capacity trend of the energy market, whether to employ a more responsive, expensive, or intermittent generations to meet the nationwide demand.

The segmentation of the electrical demand data using the clustering techniques has been introduced in order to characterise individual electrical households based on their patterns of electrical consumptions (McLoughlin, Duffy, & Conlon, 2015; Flath, Nicolay, Conte, van Dinther, & Filipova-Neumann, 2012). An example of clustering the types of demand profiles is available in (Elexon, 2016), which is based on the UK scenario. In the UK, the energy consumption from groups of consumers is classified into eight types of Profile Classes (PC) and those eight generic PCs represent the large populations of similar energy load profile characteristics within customers.

3.2.2 Modelling of demand profiles

The mathematical expression describing the demand profiles is presented, where the electrical consumption in the demand profile changes periodically with respect to time (Lau, Yang, Forbes, Wright, & Livina, 2014). Such periodical trend or time series of the electricity data should have diurnal, $D_n(t)$, and annual, $A(t)$ periodicities. The state representation of the consumed electricity signal can be generally expressed into the equation as follows:

$$X_n(t) = A\left(\frac{t}{T_1}\right) + D_n\left(\frac{t}{T_2}\right) + \varepsilon, \tag{1}$$

where $X_n(t)$ is the true state of electricity (energy consumption in kWh or MWh) at time t; $A(t)$ is the annual cycle function; $D_n(t)$ is the diurnal cycle function; T_1 is the annual periodicity, 365 days; T_2 is the diurnal periodicity, 24 hours; t is the time variable sampled at hourly rate; n indexes types of input profiles and components; ε is the signal noises. Additionally, both units of $A(t)$ and $D_n(t)$ are not limited to single unit (hours) but can be in seconds, minutes or half-hourly temporal resolutions.

The stochastic component of ε includes the following sources: (i) thermal noise; (ii) harmonic generation noise; (iii) transient noise; and (iv) frequency deviation (Lau, Yang, Forbes, Wright, & Livina, 2014). The Eq. (1) is further used as the profiling equation in developing the complete diurnal or annual trend of a demand profile representing *n*th consumer.

There are also various influencing factors affecting the overall daily demand profiles. Typical influencing factors are:

1) Seasonal variations;
2) Building characteristics;
3) Weather and temperature effects;
4) Holiday effects;

5) Consumers' consumption behaviour.

3.3 MODEL FOR PREDICTING AND ASSIMILATING CONSUMPTION PROFILES

3.3.1 Ensemble Kalman Filter

In addition to demand profiling, a good forecast technique is required in order to provide the demand forecast (days or a year ahead). Moreover, the energy demand profile usually has shown fluctuations corresponding to different time periods. This is due to the influencing factor that affects the overall energy demand across the grid. Hence, a robust, active-aware-based forecast tool is required to forecast the uncertain trends of the demand, either in long or short term forecast. To this end, the Ensemble Kalman Filter (EnKF) is applied in forecast the demand profile.

EnKF was first introduced by (Evensen, 1994) and is generally a Monte-Carlo based recursive filter approach for generation of an ensemble of model representations. An ensemble is actually a system representation through a random sampling of the system distribution (Evensen, 1994). EnKF is applied in sequential data assimilation and even a few ensemble members have the ability to exhibit large-scale covariance behaviour of a system considered (John & Mandel, 2008). EnKF is applied in the electrical systems as the resultant estimations may provide the electrical inventory for assessment of nationwide demand and energy network upgrades.

3.3.2 EnKF formulation

The formulation and description of EnKF is strictly necessary that enables the easier understanding of the demand prediction algorithm. In this case, formulations of EnKF by (Lau, 2016; Almendral-Vazquez & Syversveen, 2006; Evensen, 2003; Gillijins, et al., 2006; Jensen, 2007; Naevdal, Johnsen, Aanonses, & Vefring, 2003) are followed, with only key equations and parameters are outlined.

EnKF consists of two important steps, the *forecast* and *analysis* step. In the forecast step, as the true (actual) state is not always available, new ensemble is created in the state space by forecast the ensemble mean as the best estimate of the state (Almendral-Vazquez & Syversveen, 2006; Evensen, 2003; Gillijins, et al., 2006). In other words, a new ensemble is created based on the realisations in each of the model state through the model dynamics (simulator). It is then reflected as the first observation of the actual that will be incorporated into the model state in Eq. (2).

$$y_j^p = y^p + w_j, \tag{2}$$

where j indexes the ensemble member, y^p is the state vector of the model simulator, y_j^p is the new formation of a set of ensemble through the prediction of the model state y^p at ensemble member *j*, w_j is the model process noise. The superscript *p* denotes the priori state vector. As in line with (Almendral-Vazquez & Syversveen, 2006), the initial ensemble members of *y* are sampled from a normal distribution with the zero mean and standard deviation.

Using Eq. (1), new sets of priori ensemble y_j^p are created. Spread of the ensemble members of y are further represented into a matrix Y to denote the collection of the priori ensemble:

$$Y^p = \left[y_1^p, y_2^p, \ldots, y_j^p, \ldots, y_{N_e}^p\right], \tag{3}$$

Where N_e denotes the total number of ensemble members.

During the analysis step, new observations from measurement sets are established through ensemble representations. In order to obtain consistent error propagation, the observations have to be considered as random variables (Naevdal, Johnsen, Aanonses, & Vefring, 2003). The actual measurement is used as the reference and the random measurement noise is added to the measurement to obtain the perturbed observations (Almendral-Vazquez & Syversveen, 2006; Jensen, 2007; Naevdal, Johnsen, Aanonses, & Vefring, 2003). In this case, the actual measurement set d (also the model prediction) is perturbed using the ensemble representations, this later forms another set of ensemble of perturbed observations denoted by $d_{obs,j}$:

$$d_{obs,j} = d + v_j, \tag{4}$$

where v_j is the measurement noise at jth ensemble member. Both y_j^p and $d_{obs,j}$ are perturbed with model error: the process noise w with zero mean and covariance Q for Y^p and similarly, the measurement noise v with zero mean and covariance R for d, i.e. values w and v are assumed to be drawn from Gaussian distributions as $w \sim N(0,Q)$ and $v \sim N(0,R)$. The errors are very important to be defined in the EnKF, because without errors the system may be overspecified and no solutions resulting from EnKF propagations obtained (Jensen, 2007). The priori ensemble member y_j^p will be assimilated using the EnKF updating formula in order to obtain the updated posteriori ensemble y_j^u as follows:

$$y_j^u = y_j^p + C_p H^T (H C_p H^T + R)^{-1} (d_{obs,j} - H y_j^p). \tag{5}$$

where H is the measurement operator that relates to actual state. C_p is the priori error covariance. R is measurement covariance error. The $d_{obs,j}$ in this case corresponds to Hy_j^p. Using Eq. (5), the assimilation process is achieved by updating y_j^p, assimilating y_j^p and $d_{obs,j}$ by taking the mean of the perturbed observations $d_{obs,j}$ as the actual observation. Each of the y_j^p ensemble member is updated to obtain y_j^u. The updated y_j^u is stored into a matrix form denoted as Y^u. The product of $C_p H^T$ and $(H C_p H^T + R)^{-1}$ provides the Kalman gain. The covariance C_p can be further formulated as:

$$C_p \approx \frac{1}{N_e - 1}\left(Y^p - \overline{Y^p}\right)\left(Y^p - \overline{Y^p}\right)^T. \tag{6}$$

The root-mean-square error (RMSE) (Anderson, 2012) of the ensemble mean of y_j^u from the actual state of the model is calculated as:

$$RMSE = \sqrt{\frac{1}{k}\sum_{k=1}^{K}\left(\overline{Y_k^u} - X_k\right)^2}, \tag{7}$$

where *X* denotes the actual state of electrical consumption from Eq. (1) and *k* is the model state variable.

3.3.3 EnKF case study

This section provides the demand forecast problem using the formulated EnKF in Section 3.3.2.

In EnKF, the main intention is to estimate posteriori ensemble based on the energy consumption/demand. The initialisation of EnKF is needed by providing the model and input parameter for initial computation of the priori ensemble. Based on Eq. (2), instead of adding complex components to y^p, for simplicity the component of y^p can be formulated as:

$$y^p = \begin{bmatrix} m \\ d \end{bmatrix}. \tag{8}$$

In the simulation experiment, *m* is the model parameters of the energy consumption profile from the dynamical model Eq. (1). It is the profiling equation that describes the demand profile of *n*th consumers. As the component *m* describes the demand profile, *m* remains constant throughout the data simulation except the model process noise. This results in similar energy usage pattern from groups of consumers but with varied energy usages. The *d* is the model prediction of the energy consumption and changes with the simulation at every time step. The input component of y^p can be further extrapolated as:

$$y^p = \left[m_{1,1}, m_{2,2}, \ldots, m_{n,t}, e_{1,1}, e_{2,2}, \ldots, e_{n,t}\right]^T. \tag{9}$$

The $m_{n,t}$ refers to the component m Eq. (8) of the dynamical model from Eq. (1). The $e_{n,t}$ is the forecasted energy demand that also corresponds to the component *d*. The *n* indexes the consumer and *t* is the time step.

The `true' data of the demand profile for the mid-level grid will be further predicted using ensemble representations (denoted as actual measurement *d*), this later forms the perturbed observations ($d_{obs,j}$) based on the perturbation from *d*. Collections of y^p are stored in matrix Y^P (Eq. (3)) and are further denoted as priori ensemble (y_j^p). The y_j^p is further assimilated in the EnKF algorithm in order to obtain the new updated posteriori ensemble (y_j^u) using Eq. (5).

3.4 MODEL FOR SUPPLY BALANCING OPTIMISATION

In this section, a comprehensive holistic approach of a supply, demand and load balancing for the mid-low level grid is developed. Such model is based on the optimisation concept that aims to maximise the economic operations, and also to increase the resilience of the urban grid. The mathematical-based software optimisation module is actually developed by adapting the earlier concept from DNV GL's optimisation tool (DNV GL, 2014). The DNV GL's model is a holistic operational simulation that maximises energy economics during the normal operation, and also maximises the time for uninterrupted supply to critical infrastructures during an outage event through the power sharing mechanism in the islanding operation.

By drawing the attention to develop a holistic, complete and realistic optimisation model, the model at first simulates the demand forecast (based on individual demand profiles that are aggregated to provide overall demand across the grid), wholesale electricity market price, the initial performance/condition/committable state of distributed generators and mid-scale generating units, as well as the energy storages. In addition, there is also the need to take into account the perturbation of outage events (due to failing components, security under attacks or disasters). The outage event is needed to evaluate the capability of the grid to sustain the outage by isolating from the mid-level or low-level grid and operating in islanded mode, or by isolating grid portions and dropping the load (normal grid-connected operation for unaffected grid nodes). The ability in sustaining the islanded operation allows the evaluation of the resilience of the urban grid.

Overall, the optimisation module will enable sets of optimal designs and strategies that maximise the economic benefits through the full integration of demand profiles (end-users' behaviour of energy usage), distributed generations, mid-scale generating units, electricity connection, energy storages, and infrastructure inventory upgrades (based on the current simulation results). The model will also automatically optimise the load during grid-connected or islanded operation.

The following subsections will describe the formulation of the optimisation problem.

3.4.1 Mathematical formulation of the optimisation problem

The optimisation problem is typically the economic dispatch in the combination of unit commitment problem comprising the distributed generators and energy storages. Both problems are associated with the amount of electrical power production problems. The economic dispatch optimises the most economical way of dispatching generating units (except renewable generations), which are committable/available while meeting the nationwide demand. Details of the fuel consumption and cost function of distributed generators can be found in (Lau, 2016). In contrast, the unit commitment in the optimisation problem deals with the coordination of committable and non-committable state of distributed generators, as well as the varied loads, based on hourly interval of scheduling slots. The optimisation problem is subject to operational constraints, which will be explained in the subsequent sections.

The optimisation problem formulations from (Hedman, Ferris, O'Neill, Fisher, & Oren, 2010; Bahramirad, 2012; Saravanan, Das, Sikir, & Kothari, 2013; Khodaei, 2014a Zendehdel, Karimpour, & Oloomi, 2008) are followed. The formulation of the objective function, as well as the constraints is based on linear programming (LP) problem. This is to forbid the arising of non-linear high dimensional problems. Moreover, since the rapid optimisation solver is critical peculiarly in an emergency situation, therefore LP optimisation problem is highly recommended.

3.4.2 Objective function for normal operation

The main objective for a **normal mode** of the operation is to minimise the total operation cost as follows:

$$\text{Min } \sum_{t=1}^{NT}\left[\sum_{g=1}^{NG}\left[F_g(P_{G,gt})I_{gt} + SU_g + SD_g\right] + \sum_{s=1}^{NS}\left[C_t P_{S,st}\right] + C_t P_{M,t}\right], \tag{10}$$

where g, s and t index the corresponding generating units (thermal units), storage systems and the time period. $P_{M,t}$ is the power between the low level and the mid-level grid (the transmission line). $P_{G,gt}$ is the power dispatch of corresponding generator unit. SU_g is the start-up cost. $P_{S,st}$ is the power generated in the energy storage. SD_g is the shutdown cost. C_t is the electricity market price at the time where there exists electricity connection from the low level to the mid-level grid. I_{gt} is the binary values of commitment state of unit g. NT is the total number of time step, NS is the total number of storages and NG is generator units respectively.

The objective function in Eq. (10) is based on three important terms. The first term is the operating cost of the dispatched units. The generation cost is denoted by $F_g(P_{G,gt})$. For thermal units, the generation cost is presented in a quadratic function and is simply approximated by a piecewise linear approximation. The generator's committable/non-committable state is represented by the variable I_{gt}. I_{gt} equals to one when the unit is committable and zero when the unit is not committable. Hence, there will be a generation cost when the commitment state of the unit is one and in contrast, zero generation cost when the unit is not committed.

The start-up and shut down cost of distributed generators are also modelled explicitly. The start-up variable is introduced as u_{gt} and in contrast, the shutdown variable as w_{gt}. Both u_{gt} and w_{gt} are binary variables. When a generator unit is switched on at current time t but has been switched off until t-1, the start-up cost is imposed with u_{gt} = 1. Otherwise, u_{gt} = 0. Similarly, when the generator is switched off at current time t but has been switched on until t-1, the shutdown cost will be imposed with w_{gt} = 1 and otherwise, w_{gt} = 0. Both u_{gt} and w_{gt} has relationship with the unit commitment variable I_{gt} and can be presented as:

$$u_{gt} + w_{gt} = I_{gt} - I_{g(t-1)}, \quad (g = 1,\ldots,NG)(t = 1,\ldots,NT) \tag{11}$$

The second term deals with the energy storage. There will be cost imposed to the energy storage when the energy is stored (the energy storage is in charging mode) from the main grid at times of low electricity market prices C_t. On the contrary, during the generation (discharging mode), it is assumed that there will be zero cost imposed by energy storages.

The third term is the cost of the electricity purchased from the main grid. Depending on the state of operation, there will be electricity costs from main grid if there is an interaction between the low level grid and the main grid. In contrast, there will be zero electricity costs when there is no power drawn from the main grid.

3.4.3 Constraints

A. The power balance constraint

The power balance constraint is defined as:

$$\sum_{g=1}^{NG} P_{G,gt} + P_{M,t} + \sum_{r=1}^{NR} P_{R,rt} + \sum_{s=1}^{NS} P_{S,st} = P_{D,t}, \qquad (g=1,...,NG)(r=1,...,NR)(s=1,...,NS) \tag{12}$$

$P_{D,t}$ is total aggregated power across the grid, r indexes the renewable generating units and $P_{R,rt}$ is the power generated from renewables. The Eq. (12) ensures the total power generation from the low and mid-level local units would satisfy the overall load.

B. Unit output limits

The generation units are imposed by the minimum and maximum amount of generator capacities:

$$P_{G,g}^{\min} I_{gt} \le P_{G,gt} \le P_{G,gt}^{\max} I_{gt}, \qquad (t=1,...,NT) \tag{13}$$

where $P_{G,g}^{\min}$ is the minimum allowable capacity of $P_{G,gt}$ at generating unit g and $P_{G,g}^{\max}$ is the maximum allowable capacity of $P_{G,gt}$.

C. Ramp up and down constraints

The ramp up and down rate is formulated as:

$$P_{G,gt} - P_{G,g(t-1)} \le UR_g, \qquad (t=1,...,NT)(g=1,...,NG) \tag{14}$$

$$P_{G,g(t-1)} - P_{G,gt} \le DR_g. \qquad (t=1,...,NT)(g=1,...,NG) \tag{15}$$

UR_g is the ramp up rate limit and DR_g is the ramp down rate limit. The imposed ramping constraints limit (increase or decrease) the amount of a generating unit within two successive hours. That is to say, a generator is not allowed to reach a maximum capacity due to its nature of starting duration (hot or cold start) and the operation (Lau, 2016).

D. Transmission line capacity constraints

The transmission line capacity limit between the low and mid-level grid bus is formulated in Eq. (16). On the other hand, Eq. (17) formulates the distribution limits between low level buses.

$$\left|P_{M,t}\right| \le P_{M}^{\max}, \qquad (t=1,...,NT) \tag{16}$$

$$\left|P_{G,gt}\right| \le P_{G,g}^{\max}. \qquad (t=1,...,NT)(g=1,...,NG) \tag{17}$$

E. Spinning reserve requirement

The spinning reserve requirement is formulated as:

$$\sum_{g}^{NG} P_{G,gt}^{\max} I_{gt} + P_{M}^{\max} \geq P_{D,t} + R_t. \qquad (t=1,...,NT)(g=1,...,NG) \tag{18}$$

R_t is the reserve requirement at time *t*. The spinning reserve is the unused generation capacity which will be triggered by the central or the microgrid controller to operate the committed generators. The spinning reserve ensures the sufficient amount of generation due to imbalance in demand during an emergency situation. The R_t in this case is calculated as the percentage of the forecasted hourly load.

F. Minimum up and down time constraints

The minimum up and down time of a particular generator is defined as:

$$\left(x_{gt-1} - UT_g\right)\left(I_{gt-1} - I_{gt}\right) \geq 0, \qquad (t=1,...,NT)(g=1,...,NG) \tag{19}$$

$$\left(x_{gt-1} - DT_g\right)\left(I_{gt} - I_{gt-1}\right) \leq 0. \qquad (t=1,...,NT)(g=1,...,NG) \tag{20}$$

UT_g and DT_g is the minimum up and down time of a generating unit *g* correspondingly. x_{gt-1} is the number of hours of the generating units has been switched on (+) or off (-) .

G. Must run and off constraints

Generators are required to provide power or to switch off due at some circumstances.

$$I_{gt} = 1, \qquad (t_1 \leq t \leq t_2)(g=1,...,MR) \tag{21}$$

$$I_{gt} = 0. \qquad (t_1 \leq t \leq t_2)(g=1,...,MO) \tag{22}$$

The *MR* and *MO* indicates the *g*th unit that must run and off within the time interval respectively.

H. Contingency constraints

A *N*-1 contingency criterion is considered in the model. The *N*-1 system compliance ensures the grid can survive any single outage in any nodes, and also the line across the mid and low level grid. The generation output and the transmission line output between the mid and low level grid are constrained in the contingency situation.

$$P_{G,i}^{\min} I_{it} N1_{G,it}^{c} \leq P_{G,it}^{c} \leq P_{G,i}^{\max} I_{it} N1_{G,it}^{c}, \qquad (t=1,...,NT)(g=1,...,NG') \tag{23}$$

$$\left|P_{M,t}^{c}\right| \leq P_{M}^{\max} N1_{M,t}^{c}. \qquad (t=1,...,NT) \tag{24}$$

The superscript *c* denotes the contingency state. The index *i* refers to the generating units in *N*-1 state. $N1_{G,it}^{c}$ in Eq. (23) denotes the binary parameter for *N*-1 contingency state of the generating unit *i* at time *t*. The NG' denotes the total number of generators during the contingency event. The $N1_{G,it}^{c}$ force the *i*th generator output to be zero ($N1_{G,it}^{c} = 0$) when the generator is in contingency state and $N1_{G,it}^{c} = 1$ for normal operations. If the *i*th unit is not committable ($I_{it} = 0$), or the unit is in outage with $N1_{G,it}^{c} = 0$, the *i*th unit generation output is zero. This is to indicate that offline generator cannot respond during the contingency situation. Hence, the committable generating units are only allowed to operate in the contingency state. The operating constraints for committable generators during the contingency state will remain the same.

Similarly, $N1_{M,t}^{c}$ in Eq. (24) denotes the binary parameter for *N*-1 contingency state of the transmission line between the mid and low level grid. The $N1_{M,t}^{c} = 0$ forces the transmission flows to be zero when the transmission line is in contingency state and otherwise, $N1_{M,t}^{c} = 1$ for normal operations.

Additionally, the power balance equation from Eq. (12) changes during the contingency state. The power balance equation is therefore reformulated as:

$$\sum_{i=1}^{NG'} P_{G,it}^{c} + P_{M,t}^{c} + \sum_{i=1}^{NR'} P_{R,it}^{c} + \sum_{i=1}^{NS'} P_{S,it}^{c} = P_{D,t}^{c}. \quad (i = 1,...,NG')(i = 1,...,NR')(i = 1,...,NS')(i = 1,...,NC') \tag{25}$$

3.4.4 Objective function for islanded operation

During the islanded mode, the objective is to supply the power to critical loads from distributed generations in economic efficient manner. The objective function for the islanded operation is similar to Eq. (11):

$$\text{Min} \sum_{t=1}^{NT} \left[\sum_{i=1}^{NG'} \left[F_i(P_{G,it}) I_{it} N1_{G,it}^{c} + SU_{it} + SD_{it} \right] + \sum_{i=1}^{NS'} \left[C_t P_{S,it} N1_{S,it}^{c} \right] + C_t P_{M,t} N1_{M,t}^{c} \right]. \tag{26}$$

The *i* indexes the *i*-th generating units during the islanded operation, $N1_{G,it}^{c}$ refers the *N*-1 contingency state of the generating unit at time *t*. $N1_{S,it}^{c}$ is the *N*-1 state of the energy storage. *NG'* is the total number of generators and *NS'* is the total number of storages that are committable during the islanded operation. The operational control constraints for generators and the transmission line are remained fixed as formulated in Eq. (12)-(25).

Depending on the scale of damages to the grid during an outage event, for example, if the transmission line is not affected, i.e., $N1_{M,t}^{c}$ =1, the affected *i*th generators in a node ($N1_{it}^{c}$=0) will be in islanded mode of operation whereas the unaffected area will be in the normal mode of operation.

In order to continuously supply power to critical infrastructure during the islanded operation, the energy storage is included in the model. The modelling of energy storage is described in the next subsection.

3.4.5 Energy storage modelling

The energy storage is used often in responding to peak periods where there are rapid changes in demand. Nowadays, due to the concern in continuously supplying power during an emergency event, the energy storage has been increasingly receiving attention in mitigating the grid failures during an outage event. Henceforth, the modelling of the energy storage for the optimisation module is mandatory. The method of storage operation and modelling by (Bahramirad, 2012) is followed.

There are three important operating mode in the energy storage, which are the charging, discharging, and idle mode. For the contingency situation, the energy storage will discharge, based on the available current storage capacity.

The energy stored in a storage is the state of charge (SOC). The formulation of SOC is:

$$P_{SOC,st} = P_{SOC,s(t-1)} - P_{S,st}\Delta t, \tag{27}$$

The energy stored $P_{SOC,st}$ is the SOC of the storage, Δt is the time interval in the SOC, s indexes the energy storage.

The $P_{S,st}$ in this case is denoted with positive and negative magnitude depending the charge and discharge mode. By referring to Eq. (27), during the charging mode, the energy storage is storing the power, the $P_{S,st}$ is negative and thus the value of $P_{SOC,st}$ increases. On the contrary, during the discharging mode, the energy storage is said in generating the power and the $P_{S,st}$ is positive. Then the value of $P_{SOC,st}$ decreases. Depending on the current storage technology, some energy storage only allow the maximum discharging within half of the full storage capacity. In this case it is assumed that the modelled energy storage is allowed to discharge the power until the energy storage is completely exhausted.

The $P_{SOC,st}$ is constrained by the maximum allowable SOC ($P_{SOC,s}^{\max}$) in order to prevent overcharging:

$$0 \le P_{SOC,st} \le P_{SOC,s}^{\max}. \tag{28}$$

Another important point of the energy storage is the charge and discharge profile. By following (Bahramirad, 2012) a rectangular charging and discharging profile is assumed for the energy storage. The modelling approach of the energy storage in this case also considers the instant charging/discharging mode as soon as a charging/discharging signal is sent by a controller.

During the contingency state, the charging and discharging mode of the storage is remained the same. However, the proportion of SOC may change and Eqs. (27)-(28) are therefore modified as:

$$P_{SOC,it}^{c} = P_{SOC,i(t-1)}^{c} - P_{S,it}^{c}\Delta t, \tag{29}$$

$$0 \le P_{SOC,it}^{c} \le P_{SOC,i}^{\max}. \tag{30}$$

The operation of the energy storage is accomplished by adding the generation output $P_{S,st}$ to the power balance equation in Eq. (12). Similarly, the power balancing equation during the contingency state for storage $P_{S,it}^{c}$ is defined in Eq. (25).

The energy storage modelled stores energy at times of low energy market prices (off-peak electricity demand), and discharges the stored energy during high electricity market prices, low grid generation, and also as well as the contingency situation in compensating the generation shortages. Additionally, during the contingency state the energy storage may act as the uninterruptable power supply (UPS) that is installed in close proximity to critical infrastructures.

3.5 RESILIENCE

According to (Bollinger, 2015; Cano-Andrade, et al., 2012), the resilience is defined as the ability of a power system to recover to a new original state from an unanticipated event that causes a failure to the system. On the other hand, authors (Bollinger, 2015; Cano-Andrade, et al., 2012; Khodaei, 2014b) further extended the resilience concept by stating that resilience is the ability of a power system to withstand/remain in a state during a failure in an efficient manner, and to quickly restore to the normal operating state.

In order to access the resilience, a performance metric indicator is established. Such metric presents the extents in which the amount of energy demand within consumers are met when there is a disturbance in the grid (Bollinger, 2015). The performance metric to calculate the resiliency is based on the fraction of demand served (Bollinger, 2015; Cano-Andrade, et al., 2012).

As in line with (Bollinger, 2015; Cano-Andrade, et al., 2012), the resilience in this case is therefore the mean fraction of demand served ($P_{D,t}^{c'}$) across the outage events divided by the overall demand ($P_{D,t}^{c}$) in the contingency state:

$$\alpha_{\text{Resiliency}} = \sum_{t=1}^{NT} \frac{P_{D,t}^{c'}}{P_{D,t}^{c}}. \qquad (c = 1,\ldots,NT) \tag{31}$$

3.6 SIMULATION RESULTS

3.6.1 Numerical simulation of demand profiles

The average daily energy consumption profiles from the available public domains are adopted in examining the diurnal seasonal profiles $D_n(t)$ in the summer and winter correspondingly. The random perturbation noises are generated to indicate the signal noises as the influencing factors. Table 3-1 shows the example for types of energy consumption profiles as the input energy data included in the study.

Sector type		Sources
Household	Normal household profile (UK)	Elexon (2016)
Office	Large office (USA)	(OpenEI, n.d.)
Hospital	Large Hospital (USA)	
	Outpatient clinic (USA)	
Warehouse	Warehouse (USA)	
Supermarket	Supermarket (USA)	

Table 3-1 Types of consumer profiles included

The 2015 annual demand data from the UK National Grid portal (National Grid, 2016) is extracted and corresponds to *A(t)*. The *A(t)* obtained from the portal (National Grid, 2016) is converted to have identical temporal scale with $D_n(t)$. Using Eq. (1), those $D_n(t)$ will be 'stitched' together with *A(t)* in order to form a resultant annual trend representing the overall household demand across the grid (Lau, Yang, Forbes, Wright, & Livina, 2014). It is intended to demonstrate only the demand profile of household in this section, as the full profile of other sectors are demonstrated in the low level tool section 4.5.

Figure 3-3 shows diurnal energy consumption profile for domestic households during summer and winter seasons. Based on Figure 3-3, it can be seen that a household electricity consumption drops during the working hours and maximum demand occurs during the peak period (1700-1900). Additionally, the amount of energy consumption during the winter is much higher than other the summer season due to the high amount of heating.

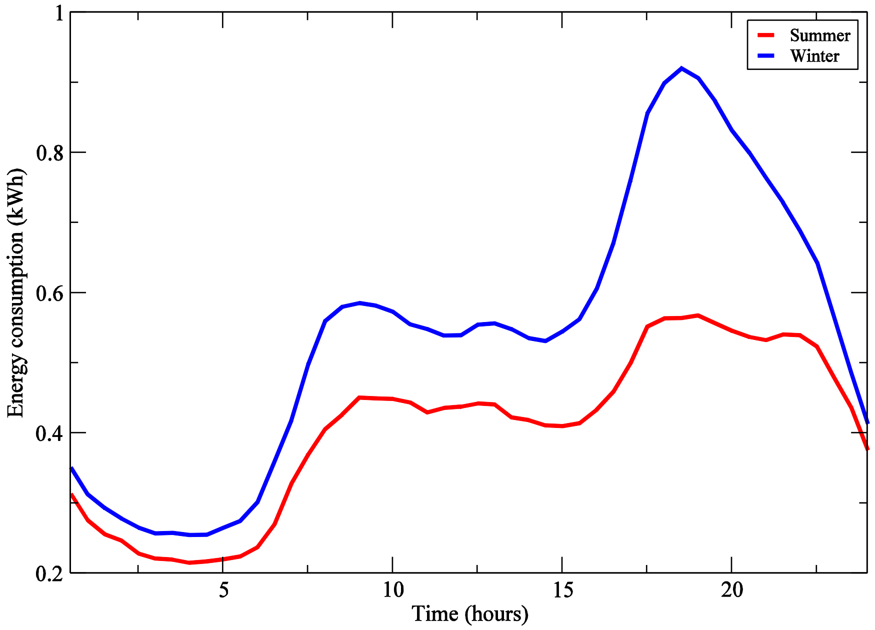

Figure 3-3: Diurnal energy consumption (demand) cycles for the UK domestic household.

The result plot of the average daily annual energy consumption is shown in Figure 3-4, where $D_n(t)$ is stitched with *A(t)* that forms the complete annual household demand trend. The estimated annual energy consumption is 4023kWh and such estimated value is similar to the overall household energy consumption usage as reported by the UK Department of Energy and Climate Change (DECC, 2014). Henceforth, the developed household energy demand trend is a good representation profile for the domestic household consumers.

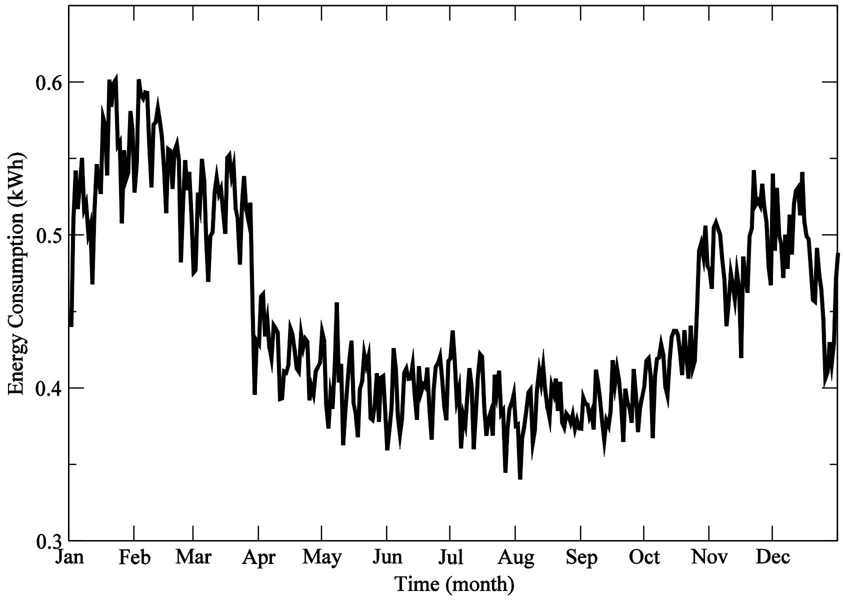

Figure 3-4: Average daily annual energy consumption (demand) profile for the UK domestic household.

3.6.2 EnKF numerical simulation

The EnKF simulation in this case involves short-term based day ahead forecast and assimilation of the energy consumption profiles from Table 3.1. Samples of consumers from the respective sector are: 10000 households, 2 large offices, 2 large hospitals, 5 outpatient clinics, 5 supermarkets, and 5 warehouses. They are created individually with the addition of model noises in order to reflect forecast energy usages among groups (some variations of energy usages within the same group). The modelled profile of $X_n(t)$ from Eq. (1) is the observation that reflects the actual system that will be incorporated into the model state in Eq. (8). Since the demand data is available as illustrated in Table 3.1, variable y^p in Eq. (8) contributes to direct model predictions (*d*) of the energy demand (based on the Eq. (1) that formulates the demand profile (*m*)).

The priori ensemble y_j^p is created using Eq. (2), where $j = 1, ..., N_e$. As in line with (Lau, 2016), initial ensemble members of y^p are intended to be drawn from a normal distribution with the mean and standard deviation $N(0, 20)$. Additionally, the model error w is sampled from $w \sim N(0, 1)$. The measurement error v, on the other hand, is sampled from $v \sim N(0, 0.5)$.

In the EnKF, the perturbed observation of demand data $d_{obs,j}$ is based on the model prediction d using Eq. (4). Different realisations (N_e = 10, 50, 100, 500, 1000) are created and propagated at every time steps. The Y_p in Eq. (3) is the collection of the priori ensemble y_j^p, which is assimilated along with $d_{obs,j}$ and updated to form the posteriori ensemble y_j^u through Eq. (5).

The posteriori ensemble mean distributions of the energy demand with different realisations N_e are computed that allow comparison of the convergence in relation to the true (actual) state of the model. The RMSE of the propagated ensemble mean in relative to the actual model state is calculated using Eq. (7), in order to examine the robustness of EnKF in different realisations.

As mentioned, a day head with hourly temporal resolution is adopted to demonstrate the resultant EnKF propagations. The input data from Table 3.1 is applied and aggregated in order to tabulate the overall demand from the individual profile (Eq. (1)) across the grid as follow:

$$X_{Total}(t) = \sum_{n=1}^{N} X_n(t). \quad (32)$$

The diurnal plot with datasets of the actual energy demand and propagation of Y^u with different ensemble sizes is shown in Figure 3-5. The summer profile for the energy demand is included only in the report as the overall trend of the winter profile is similar with the summer profile (with the magnitudes as the only main difference). The figure shows that the larger the ensemble size, the better Y^u estimation converges towards the actual energy demand.

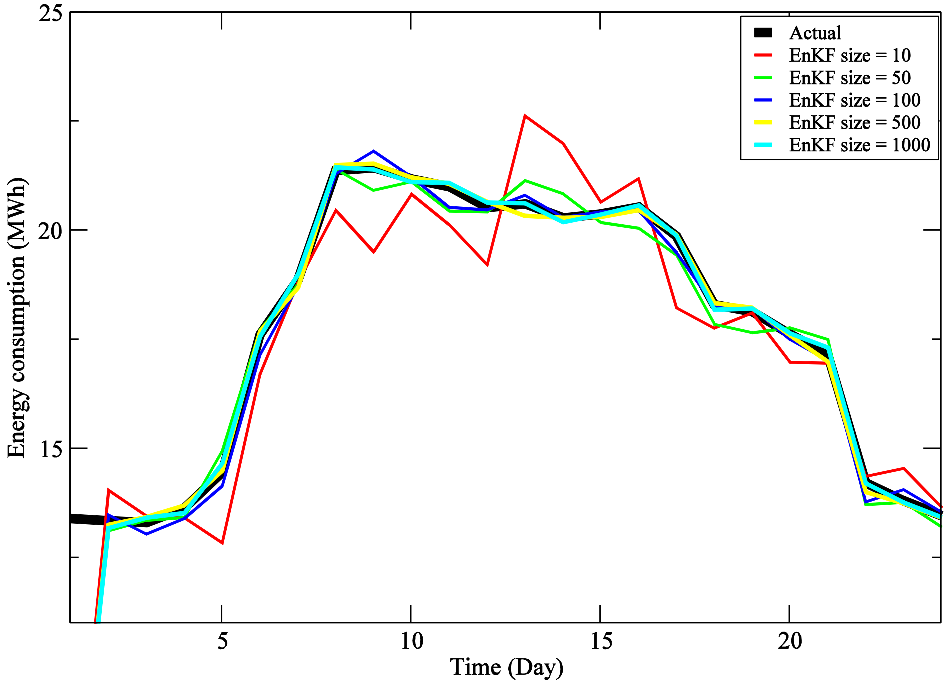

Figure 3-5: Diurnal energy consumption profile with different EnKF realisations.

Similarly, it is the main intention to illustrate the EnKF forecast for few days ahead. Figure 3-6 shows the extended five days plot of actual observation of energy consumption and propagation of Y^u with different ensemble sizes. The figure also reflects that the larger the ensemble size, the better Y^u estimation converges towards the actual energy consumption data.

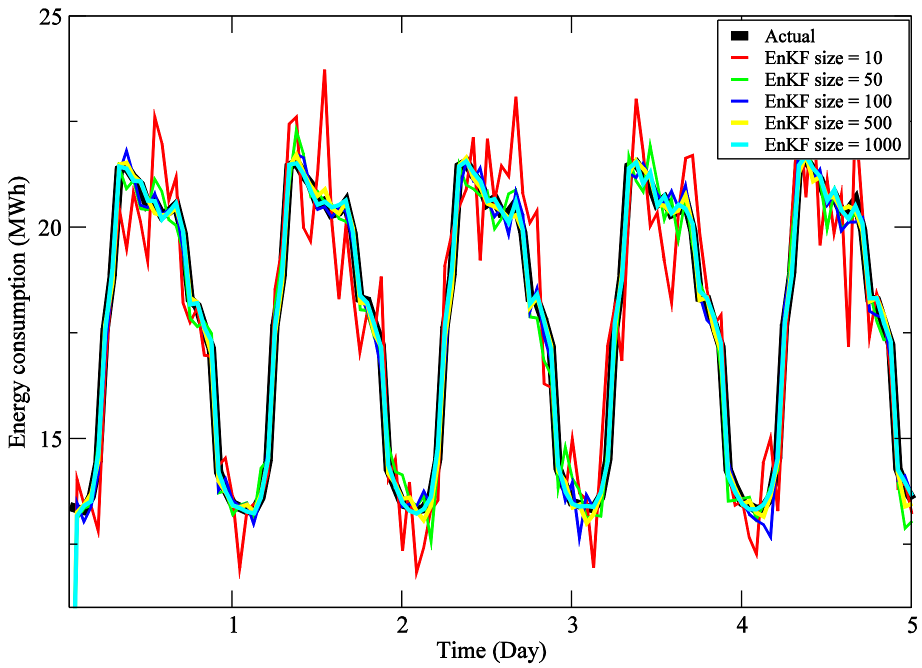

Figure 3-6: Five days energy consumption profile with different EnKF realisations.

The tabulated RMSE values corresponding to different EnKF realisations are shown in Table 3-2. The RMSE values from Table 3-2 also indicate that the larger the ensemble size, the smaller the RMSE value, and hence the better the EnKF estimations.

Number of ensemble (N_e)	RMSE value
10	2.1793
50	1.0469
100	0.5545
500	0.2339
1000	0.1749

Table 3-2 The RMSE value with different EnKF realisations

Both EnKF simulations demonstrate that the EnKF realisation of N_e = 500 is sufficiently enough to provide accurate forecasts. The simulations also exhibit the robustness of EnKF in forecast and matching the energy demand.

The resultant energy consumption profile is further applied in the optimisation module as the overall energy demand across grid ($P_{D,t}$).

3.6.3 Optimisation

The IEEE 14-bus system representing the grid topology from Figure 3-2 is applied in examining the overall operation of grid during the normal and islanded mode of operation. Samples of consumers from the respective sector (10000 households, 2 large offices, 2 large hospitals, 5 outpatient clinics, 5 supermarkets, and 5 warehouses) from the previous EnKF based results are used. The generations and load distributions of the grid are shown in Table 3-3.

Bus No.	Number of distributed generators		Number of energy storage	Profiles included	Type of voltage
	Non-renewable	Renewable			
1	2	2	2	Households	Low voltage
2	3	2	2	Large offices	Low voltage
3	4	1	2	Hospitals	Low voltage
4	2	0	2	Outpatient clinics	Low voltage
5	2	1	2	Supermarkets	Low voltage
6	2	0	2	Warehouses	Low voltage
7	1	0	2	0	Medium voltage
8	0	0	2	0	Medium voltage
9	0	1	0	0	Medium voltage
10	0	1	0	0	Medium voltage
11	0	0	0	0	Empty voltage
12	0	0	0	0	Empty voltage
13	0	0	0	0	Empty voltage
14	0	0	0	0	Medium voltage

Table 3-3 Number of distributed generators, energy storages, types of consumer profiles and their loads included.

Based on Table 3-3, buses (nodes) 1-6 consist of the main distributed generation buses and the loads, while buses 1-8 contain the energy storages for reserving purposes, buses 11 – 13 contain empty generation and load sources. Finally, Bus 14 is the connection to the main grid. The distribution of load profiles in this case is not intended to include the profiles of commercial services (e.g. hospitals, offices) and domestic households within the same bus. However, the variety of commercial services within a same bus is still possible. Additionally, most of the commercial services are connected with their own substation due to the huge amount of loads required.

Additionally, it is not the priority and the scope in evaluating the excess/surplus generation that can be sold. The model and the scenarios created aim to evaluate the overall performance of the grid in responding to contingency events.

The characteristic of renewable distributed generations applied in this case is presented in Table 3-4 (a) for small-scale renewable & (b) for mid-scale renewable generators (Jayaweera & Islam, 2014).

Unit number	Units installed (buses)	Minimum capacity (kW)	Maximum capacity (MW)
R1	1,2,3,5	0	2
R2	5	0	0.5

Table 3-4 (a) Characteristics of renewable generations (small scale)

Unit number	Units installed (buses)	Minimum capacity (kW)	Maximum capacity (MW)
R3	9	0	2.0
R4	10	0	0.6

Table 3-4 (b) Characteristics of renewable generations (mid scale)

Table 3-5(a) & (b) show the specification of (a) small scale non-renewable generator; (b) mid-scale non-renewable generator. The specification data in Table 3-5 (a) & (b) was originally adopted from (Bahramirad, 2012; Lau, 2016), with some implemented modifications in fitting the required generations to the load demands.

Unit number	Units installed (buses)	Cost of generation (£/MWh)	Minimum capacity (MW)	Maximum capacity (MW)	Start-up cost (£)	Shutdown cost (£)
Gen 1	1,3,4	27.1	0.1	10	40	3
Gen 2	2,3,5,6	39.1	0.1	10	40	3
Gen 3	2,3,4,5,6	61.3	0.5	5	10	0
Gen 4	1,2,3	65.6	0.5	5	10	0

Unit number	Minimum up time (hours)	Minimum down time (hours)	Ramped up rate (MW/hour)	Ramped down rate (MW/hour)
Gen 1	3	3	2.5	2.5
Gen 2	3	3	2.5	2.5
Gen 3	1	1	3	3
Gen 4	1	1	3	3

Table 3-5 (a) Characteristics of non-renewable generations (small scale)

Unit number	Units installed (buses)	Cost of generation (£/MWh)	Minimum capacity (MW)	Maximum capacity (MW)	Start-up cost (£)	Shutdown cost (£)
Gen 5	7	170	0.5	20	50	10
Gen 6	9,10	133	0	20	50	0

Unit number	Minimum up time (hours)	Minimum down time (hours)	Ramped up rate (MW/hour)	Ramped down rate (MW/hour)
Gen 5	5	2	5	5
Gen 6	2	2	5	5

Table 3-5 (b) Characteristics of non-renewable generations (mid-scale)

According to (Lau, 2016), as the renewable generation is intermittent, other conventional generators (thermal units and hydro) are used primarily to balance the renewable output. The integration of conventional generators with the renewables ensures sufficient amount of energy output that satisfies the energy demand. The renewables are generally assumed to be uncontrollable in adjusting the required load factor. Hence, there is no associated optimisation performed in the renewables.

According to (NYSERDA, DPS, & DHSES, 2014), the grid cannot fully depend on renewable energy resources during contingency states with the level of security required for contingencies. Additionally, the need to provide enough power to critical infrastructures during the islanding mode may require the redundant generators to protect against the failure of one or more generators (NYSERDA, DPS, & DHSES, 2014). Therefore, there must be at least two generators installed in each node with electrical loads, where there must be also at least one generator that are committable in responding to contingency situations.

Furthermore, authors (NYSERDA, DPS, & DHSES, 2014) added that the characterisations of distributed generations, whether it is for the contingency, base load, or intermittent generations must be implemented. Typical characterisation is provided by (NYSERDA, DPS, &

DHSES, 2014) such as: contingency generators: Diesel generators; base load generators: CCGT; Intermittent generators: wind and solar. In this case, the contingency generators include the energy storages and generators (Gen 3, 4 and 5), base load generators include (Gen 1, 2 and 6), and intermittent generators such as (R1 - 4).

For the energy storage, two identical units with the total of 500 kWh storage capacity (250 kWh each) are included in the simulation. Each of the storage can be charged at the rate of 0.25 MW/hr within 8 hours in order to reach the maximum SOC of 4 MWh. The energy storage can be charged when the capacity is either partially or completely depleted. All energy storages will be charged at times of low electricity price and discharge during the peak periods, and also during the contingency situation. In this case, it is assumed that the energy storage will generate power at the time 1700 daily for the duration of four hours.

The 2015 average electricity market price data is shown in Figure 3-7. The wholesale data is obtained from the portal (APX Power Spot Exchange, 2016a). It is one of the UK's power exchange providing the trading and clearing services for the wholesale market (APX Power Spot Exchange, 2016b). The portal (APX Power Spot Exchange, 2016a) provides historical data of reference price data for the electricity. The 2015 year of reference price data is adopted, with additional calculation to perform the average daily whole electricity price data. In addition, the 2015 mean wholesale electricity price data is shown in Table 3-5.

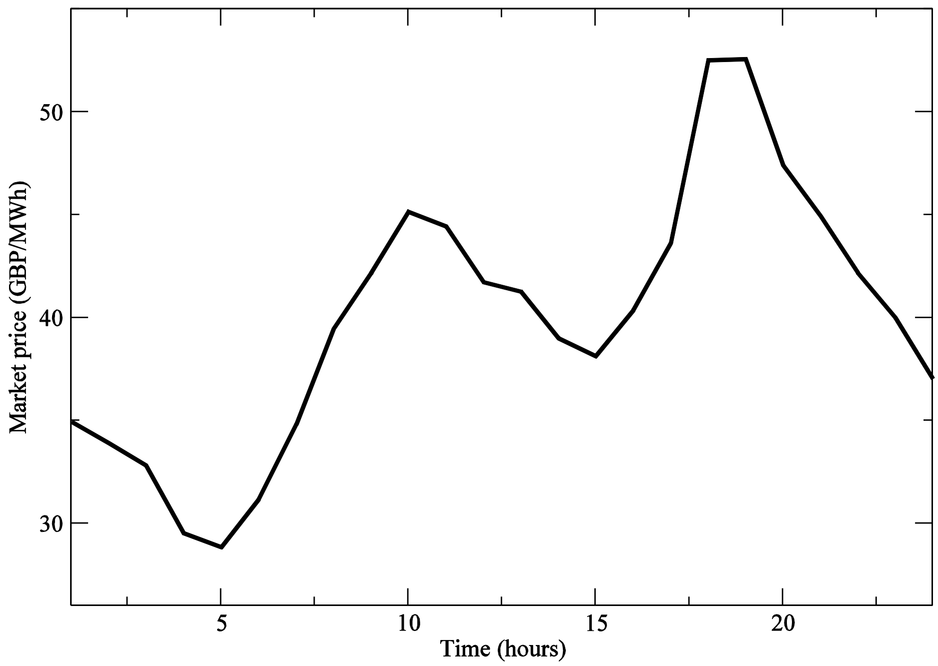

Figure 3-7: The 2015 average electricity market price data. Source (APX Power Spot Exchange, 2016b).

Hour	1	2	3	4	5	6	7	8	9	10	11	12
Price (£/MWh)	34.94	33.90	32.82	29.54	28.86	31.19	34.83	39.47	42.17	45.16	44.46	41.74
Hour	13	14	15	16	17	18	19	20	21	22	23	24
Price (£/MWh)	41.28	39.02	38.14	40.38	43.63	52.52	52.57	47.41	44.95	42.19	40.02	37.05

Table 3-5 The average 2015 electricity price market data

Prior to the optimisation, as in line with (Bahramirad, 2012), all the generating units are switched off initially. However, the minimum down time limit has been achieved by all units, therefore the units can be switched on at the first time step. The demand from each node will be summed in order to provide the total aggregated demand across the grid ($P_{D,\,t}$). The time-line for the simulation is limited to 24 hours with the hourly-based temporal resolution. As the time interval for the optimisation is 1 hour, the Δt in Eq. (27) and (29) is set to $\Delta t = 1$. The *N*-1 contingency criterion is applied in the ensuring the effectiveness of the grid in sustaining a single outage event.

The optimisation is solved using the Matlab software. The dual-simplex algorithm is applied for this LP problem of the grid optimisation. The business-as-usual case of the grid operation is simulated, along with the optimised solution. The electricity price threshold in this case is adjusted to £45.5/MWh. This allows the interaction between the mid-level and low-level grid in responding to the market price. When the market price is generally cheaper than the cost of generating units in the local units, the power will be purchased from the main grid (high and mid-level grid). Then, the grid-connected operation is applied where low level load is fully supplied by the main grid. On the other hand, the generating units will operate to provide microgrid load, instead of drawing the electricity from the main grid when the electricity price is high.
It is important to note that we distinguish between a deliberated and an emergency islanding operation, where in the first case a so-called ‘economic-based islanding operation’ is triggered to prevent the low level grid from drawing the electricity from the main grid at times of high electricity price.

A total of three different scenarios are created to illustrate the effectiveness of the grid operation. After the completion of the simulation, the performance of the grid is evaluated in terms of the cost savings, and the overall resiliency of the studied grid.

3.6.3.1 Scenario 1 – Normal grid-connected operation and economic islanding

In the first scenario, there is no outage in the system and hence the business-as-usual grid-connected mode of operation is applied. The energy demand distributions corresponding to different nodes, and also the total energy demand across the grid are shown in Figure 3-8. It can be seen that the Node 3 consisting of the component of large hospitals contributes the highest amount of energy consumption.

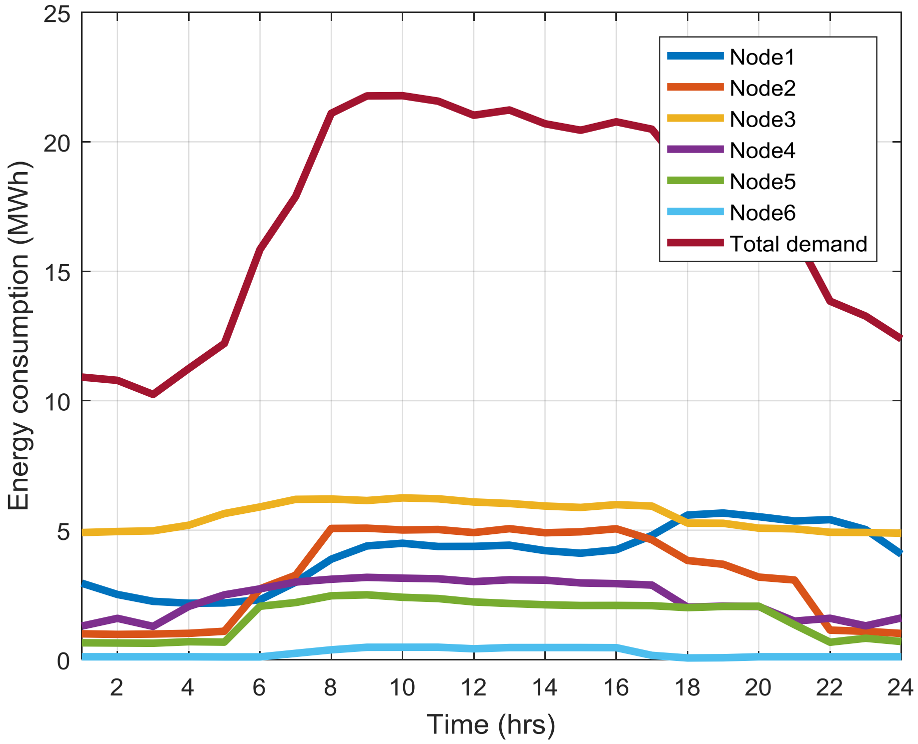

Figure 3-8: The energy demand distributions corresponding to each node, and also the total demand across the Microgrid.

Additionally, the total energy demand at every time interval is large (>10 MW than a standard microgrid capacity). This is due to the huge loads contributed by large hospitals and offices. Such configuration of the grid in this case is, however, not limited to small loads. The low voltage grid configuration depends on the variation of loads, the spatial scale of the consumer groups and specifications of generating units.

The resultant plot of the demand and the balanced demand is shown in Figure 3-9. The legend *'Balanced demand'* in Figure 3-9 denotes the optimised demand based on the resultant summation of demand across each nodes. The overlapped lines (particularly Node 1 – Node 6) in Figure 3-9 denote the amount of energy generation that corresponds to the overall demand across the grid ($P_{D,t}$). Additionally, the legend *'Demand'* is denoted as $P_{D,t}$. Therefore the summation of *'Balanced demand'* across each nodes equals to $P_{D,t}$ as in Eq. (12). When the electricity price is low (at hours 0 – 18), the normal grid-connected mode is in operation where the power is actually imported from the main grid to the low-level grid. During the times of high electricity price, non-renewable units and energy storages in low level grid are triggered by the microgrid controller, along with the on-running renewable systems to generate power in order to satisfy the current load. At these instance, the microgrid is in *islanded* mode of operation and there is no power purchase from the main grid. After that, when the electricity price is low (at hours 20 – 24), the islanding mode operation terminates and the normal mode of grid-connected operation occurs. It is also assumed that the grid applied in this case has the capability to cut the power from the grid entirely due to the sophisticated design and capability of CBs.

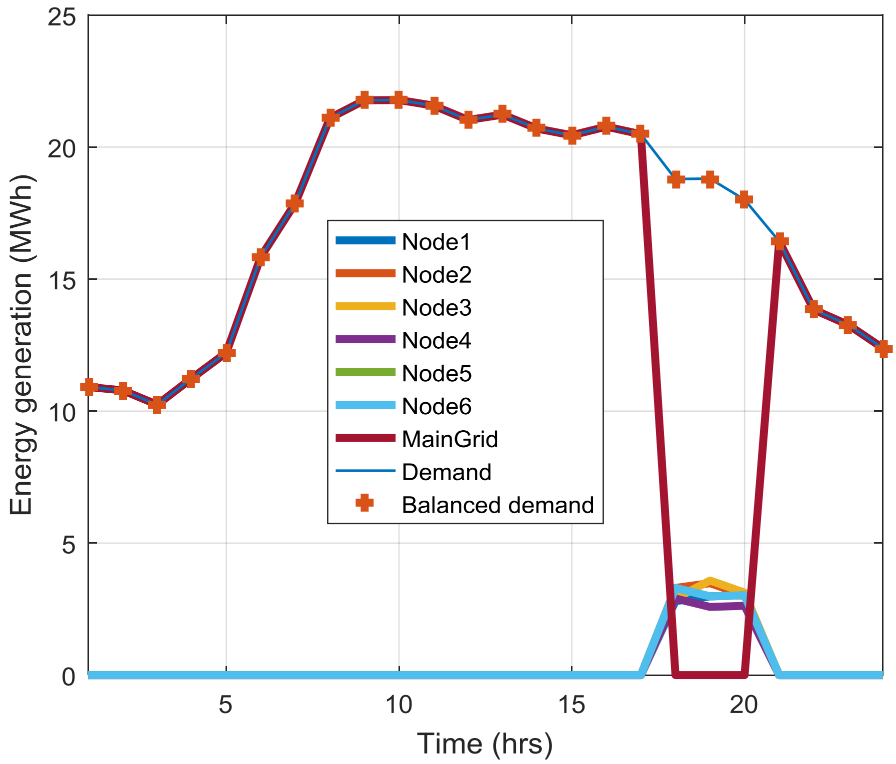

Figure 3-9: The energy demand distribution and its balanced demand through optimisation corresponding to each node and the main grid.

Due to the high amount of generators involved, it is not feasible to illustrate the generation output for corresponding generators in each node. All the generating units are strictly constrained by the operating conditions in order not to breach the maximum allowable operational standards, based on the outlined constraints earlier.

In this example, as the islanded operation of the grid is price-triggered, it is not an *N*-1 based contingency situation, hence the resiliency index in this case is zero. This scenario is deliberately introduced in examining the capability of the grid in controlling the amount of distributed generation outputs in responding to the electricity market price.

The operating state and the SOC of the energy storage are shown in Figures 3-10 and 3-11.

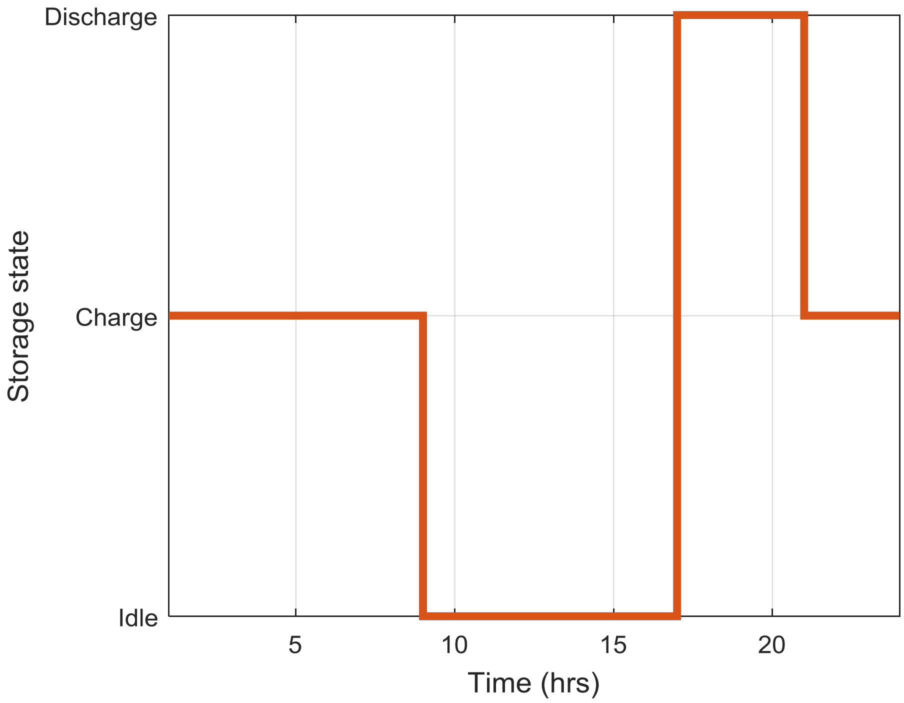

Figure 3-10: The operating state of the energy storage.

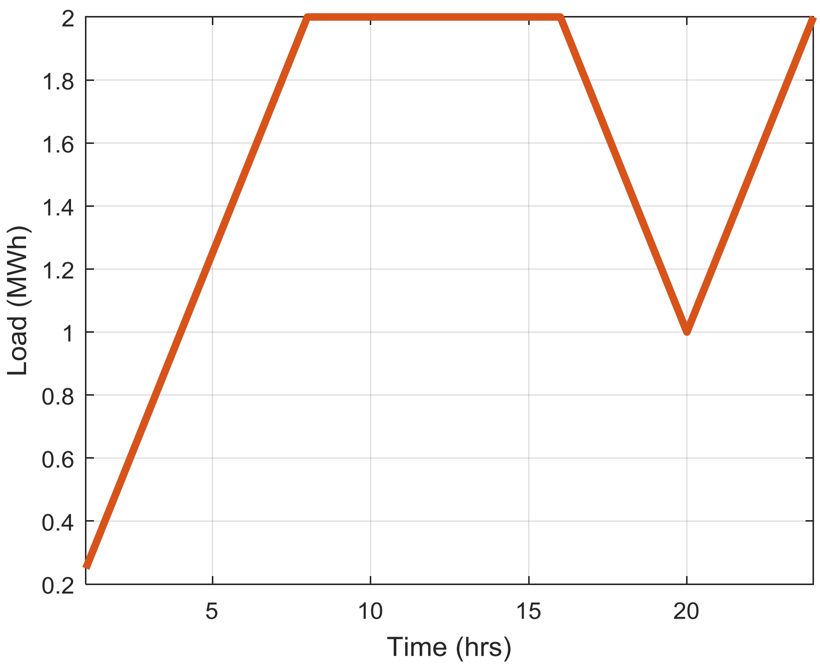

Figure 3-11: The state of charge in the energy storage.

Based on Figures 3-10 and 3.11, the energy storage is charging to its full capacity at times of low electricity price. The duration of charging is 8 hours and the storage will be in 'idle' mode, (maximum state of charge of 2 MWh) awaiting the generation instruction. At time of peak period (at hours 17 – 21), the storage generates (discharging) power to the grid (either mid or low-voltage level). Then the storage will begin to charge again at times of low electrical price (from hours 21 onwards), in order to prepare for the next stage of scheduling horizon. Furthermore, the energy storage is not required to be fully depleted to allow for charging, instead the charging mode can be triggered as soon as cheap electricity price occurs.

The cost of operation for the business-as-usual and optimised whole grid solution is shown in Figure 3-12. In this case, the business-as-usual is defined as when only grid-connected mode of operation is allowed. In contrast, the optimised grid solution is when there are both grid-connected and islanded operations as illustrated in Figure 3-9. The overall cost saving in this 24 hours of simulation runs is £1724.30 (see for a comparison the concluding section 5). Hence the first scenario shows the positive aspects of the grid in avoiding the purchase of high-electricity price from the main grid. The capability of the 'economic-islanded' operation at times of peak electricity price shows the robustness feature of grid in optimising the cost of dispatchable units. The cost saving calculated in this case excludes the other factors such as the maintenance and other overhead costs from the respective renewable and non-renewable generators, and the energy storages.

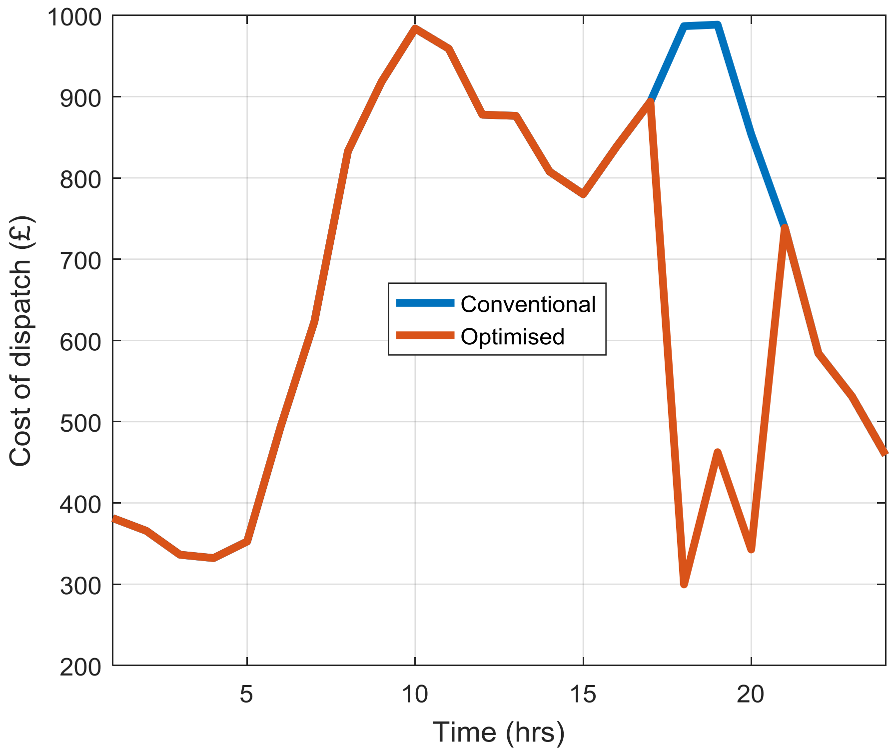

Figure 3-12: The cost of operation between the business-as-usual and optimised solution.

3.6.3.2 Scenario 2 – Islanded operation due to the failure of one power generation node

In this second scenario, it is assumed that one of the generator (labelled as Generator 1) in Node 3 is in the contingency state (outage) and therefore the Generator 1 associated to Node 3 is isolated from generation. The outage starts at 09:00 for the duration of six hours. Therefore, the needed demand in Node 3 is obtained from either rest of the generating units. The grid, similar to Scenario 1, will still be in the normal mode of operation. The electricity price threshold and all other configurations of generating units are remained the same. The economic-islanded operation remains at times of high electricity price (provided that there is no outage during these intervals) as shown in the previous scenario.

Figure 3-13 illustrates the overall energy generation of corresponding generators, energy storages and renewable in Node 3. From Figure 3-13, due to the outage in Generator 1, the Generator 1 is not committable from 09:00 to 14:00. Other forms of generating units, including energy storages (controllable) and renewable (not-controllable) are employed to balance the remaining outputs from Generator 1. The energy storages (Storage 1 and 2) discharge (generate power) when the outage event occurs, and stop discharge when the Generator 1 is brought back online at hours 14:00. Additionally, it can be also seen that contingency based generators (Generator 3 and 4) are employed to handle the outage event.

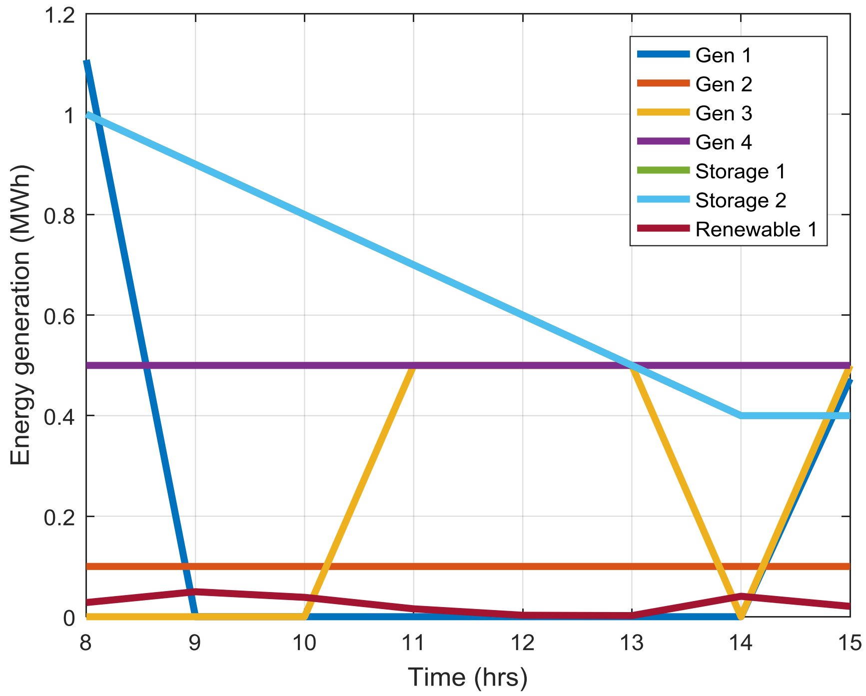

Figure 3-13: The energy generation distribution of corresponding generators, energy storages, and renewables in Node 3.

The operating state and the SOC of the energy storage for Node 3 are shown in Figures 3-14 and 3-15.

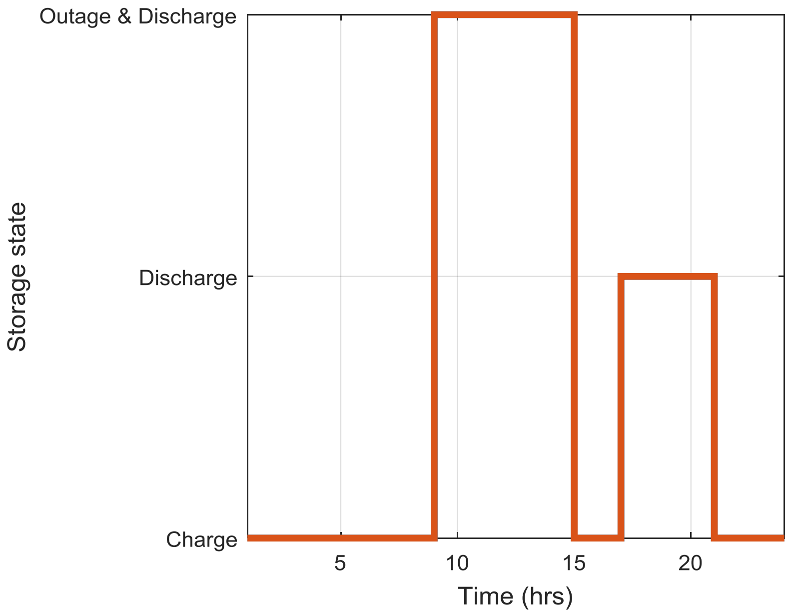

Figure 3-14: The operating state of the energy storage in Node 3.

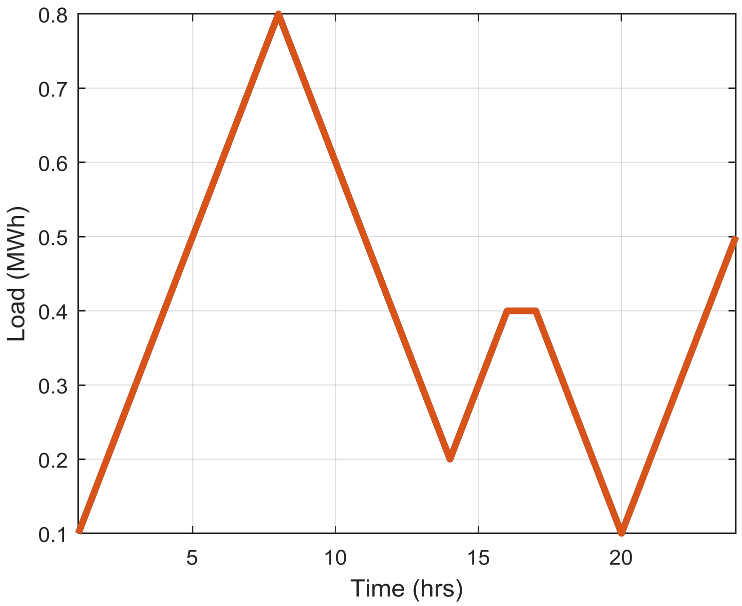

Figure 3-15: The state of charge in the energy storage in Node 3.

Based on Figured 3-14 and 3-15, the energy storage is charging to its full capacity at times of low electricity price. At time of outage in Generator 1 (at hours 9 – 14), the storage generates power to compensate the imbalances of Node 3 due to the Generator 1 failure. At hours 15, as the outage is solved and additionally, the electricity price is low (below the electricity price threshold), the storage is allowed to charge. Then during the peak period (at hours 17 – 21), similar to the first scenario, the storage will again generate power for the peak period. Finally, the storage will begin to charge again at times of low electrical price (from hours 21 onwards), in order to prepare for the next stage of scheduling horizon.

The cost of operation for the business-as-usual grid and optimised microgrid solution is shown in Figure 3-16. The overall cost saving in these 24 hours of simulation runs is £ 1850.80. Hence the second scenario shows the positive aspects of the grid in the capability of operating in the contingency state.

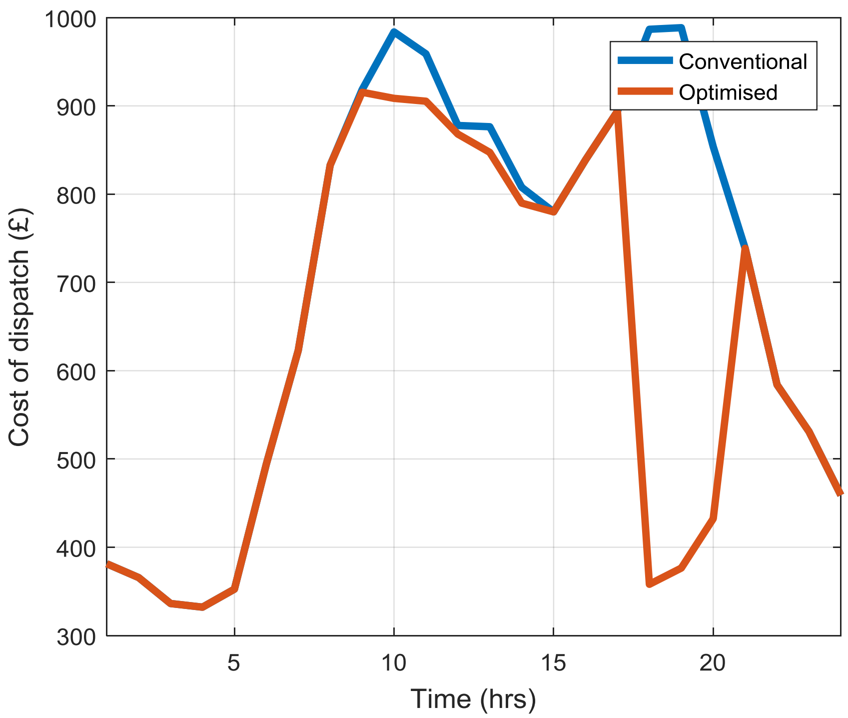

Figure 3-16: The cost of operation between the business-as-usual and optimised solution during the outage in Node 3.

The resilience distribution of the Node 3 due to the broken Generator 1 is shown in Figure 3-17. It can be seen that from Figure 3-17, the resilience during the outage is average-high. The zero percentage of resilience indicates the normal state of grid operation. Using Eq. (31), the overall resiliency of the system is calculated as 0.29. Such calculation demonstrates the capability and resiliency of the grid to withstand the generator outage in an efficient manner, and to restore to the normal operating state quickly. In contrast, that if there is a huge amount of loads deviated during the outage, and the resultant resiliency calculated is very low, this indicates the low resiliency of the grid in sustaining the required loads.

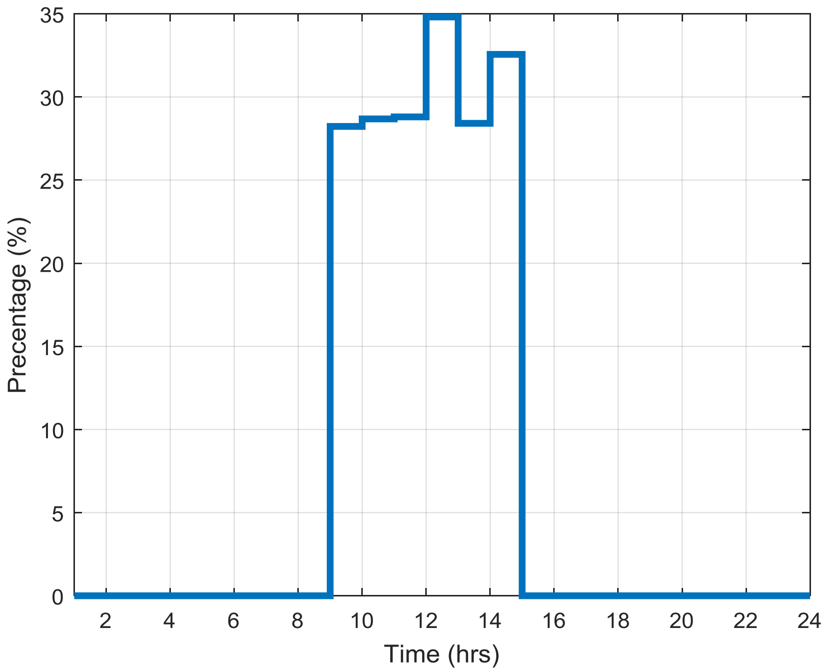

Figure 3-17: The resilience distribution of the Node 3 during the outage in Generator 1.

3.6.3.3 Scenario 3 – Islanded operation due to the outage in the mid-level grid

The third scenario accounts the outage of the mid-level grid. Similar to the second scenario, the mid-level grid outage starts at 09:00 for the duration of six hours. During the grid outage, islanded mode of grid operation for the low level grid is achieved. The electricity price threshold and all other configurations of generating units remained the same.

Figure 3-18 illustrates the overall energy demand distribution and its balanced demand, following the outage in the main grid. Similar to Figure 3-9, the legend *'Balanced demand'* in Figure 3-18 denotes the optimised demand based on the resultant summation of demand across each nodes during the contingency state. Additionally, the legend *'Demand'* denotes the overall demand across the grid ($P_{D,t}^{C}$). Therefore the summation of *'Balanced demand'* across each nodes equals to $P_{D,t}^{C}$ as in Eq. (25). From Figure 3-18 it is notable that due to the outage in the mid-level grid, the mid-level grid load drops to zero at hours 9 – 15. Therefore, all nodes in the low-level grid operate in islanded mode. As the outage event terminates, the all nodes terminate their islanded operation, re-connect to the main grid that permit the grid-connected mode of operation. In this example, the economic-islanded operation of the grid is also introduced at times of high electricity price (provided that there is no outage during these intervals).

The cost of operation for the business-as-usual grid and optimised grid solution for the third scenario is shown in Figure 3-19. The overall cost saving in this 24 hours of simulation runs is £5007.28 (see costs saving summary in Section 5). Hence the third scenario also shows the positive aspects of the grid in isolating the operation during the mid-level grid outage.

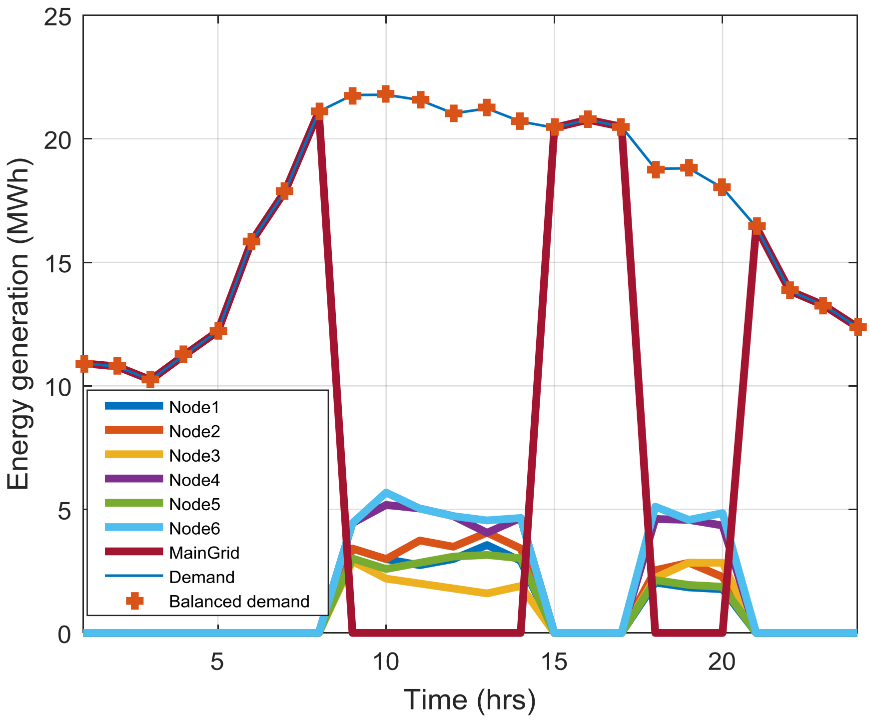

Figure 3-18: The overall energy demand distribution and its balanced demand corresponding to each node and the main grid following the mid-level grid outages.

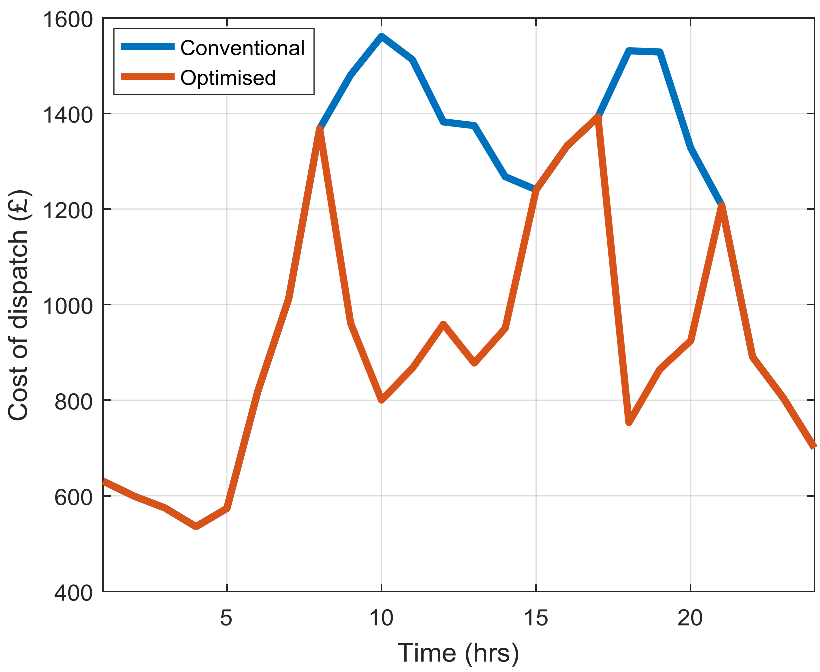

Figure 3-19: The cost of operation between the business-as-usual and optimised solution during the outage in the mid-level grid.

The resilience distribution of the microgrid is shown in Figure 3-20. It can be seen that from Figure 3-20, the resilience is at the highest point. This is due to the mid-level grid outage that requires the complete contribution of islanding operation from the low-level grid. Additionally, the overall resiliency of the system is calculated as 1. Such calculation demonstrates the capability and resiliency of the microgrid to withstand the outage. In contrast, if the resiliency is not tabulated as 1, this indicates that there are portion of demands that fail to be served during the outage event. Thus the overall resiliency of the grid in sustaining the required loads is affected.

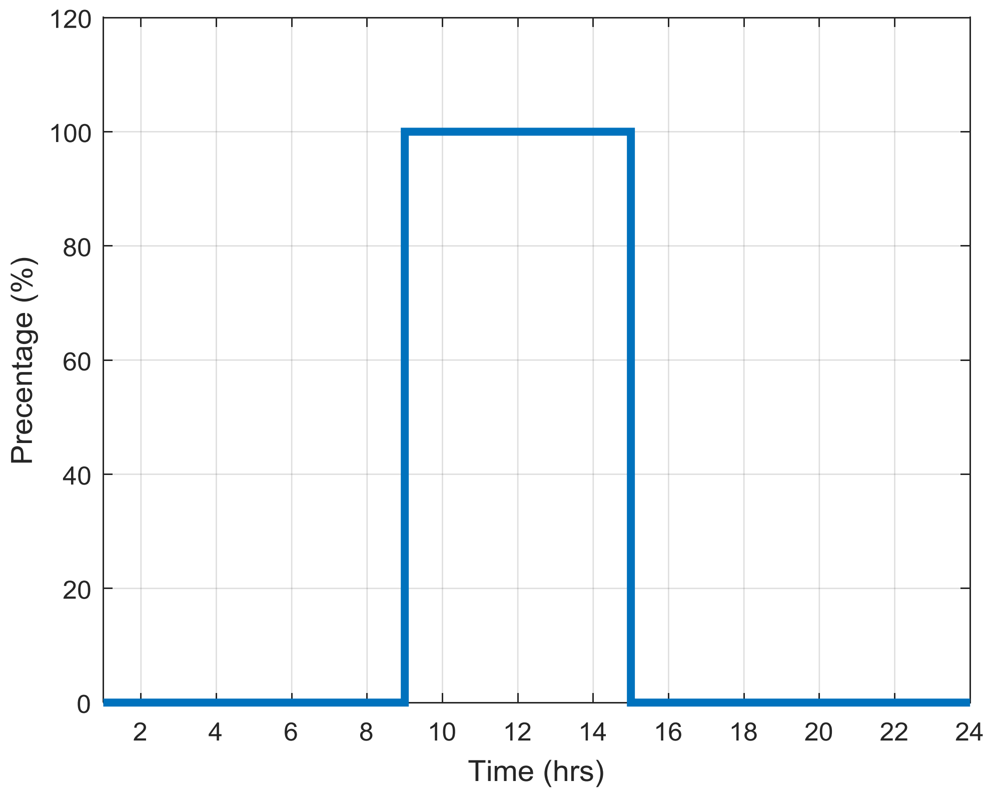

Figure 3-20: The resilience distribution of the grid during the mid-level grid outage.

4 OUTAGE RESPONSE USING DEMAND SIDE MANAGEMENT (DSM)

In this chapter we investigate the use of DSM for energy management (EMS) in normal and islanded mode. The Demand Side Management consists of mechanisms to change the energy consumption behaviour of users using a) energy price incentives or b) allowing direct load control of user assets. In the latter case the user is rewarded with a discounted energy contract.

In our case the goal of EMS is to optimize the energy consumption taking into account the existence of flexible loads, photovoltaic (PV) generation and battery storage.

Demand side management (DSM) in microgrids with flexible loads, distributed generation (DG) and storage has been already addressed previously in (Lopes, 2009), (Olivares, 2014). However, few works have studied the impact of flexibility information exchange and the DSM effect on the microgrid operation during long lasting outages.
Using the classification in (Olivares, 2014), we focus on a secondary control centralized architecture, in which the time horizon is minutes up to hours, therefore - significantly larger than for primary control systems.

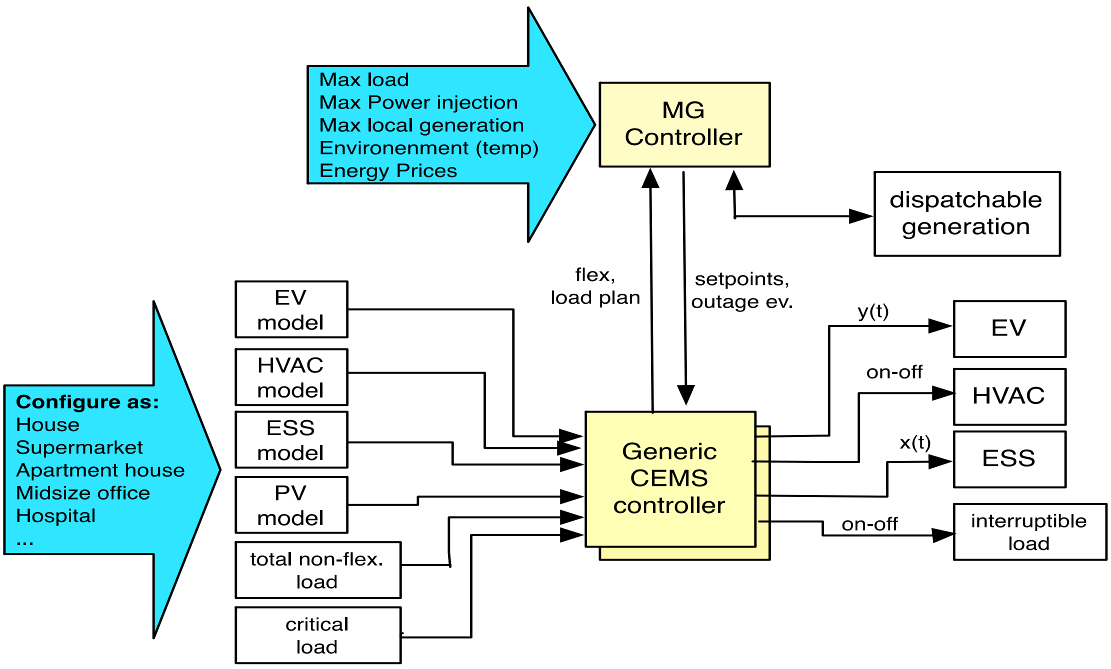

Figure 4-1 Microgrid component architecture

Figure 4-1 illustrates the generic flexible assets that can be attached to each CEMS, such as HVAC, electric vehicle (EV), Battery storage (ESS), or PV generation. With these ingredients and the appropriate consumption/generation profiles, different buildings can be configured as part of the microgrid loads.

For the realisation of the control loop, the Model Predictive Control (MPC) technique (Parisio, 2014) is used, meaning that the power consumption (and generation) is predicted for a certain time horizon (e.g., six hours), however the actuation is performed only for the next period.

The MPC mechanism is combined with a novel exchange of flexibility information. Energy flexibility is defined for assets such as HVAC (heating, ventilation, air conditioning) electric vehicle charging or battery storage. Each CEMS controller aggregates the flexibility of its assets and reports the resulted profile (for the next six hours) together with the planned consumption profile. The latter is the result of an optimization step, taking into consideration local goals, MG setpoints and constraints from all the local assets.

The MG controller reads the latest flexibility and consumption plans from the CEMS and computes updated setpoints (also six hour profiles). In case the proposed consumption is too high, it sheds certain demands within their flexibility limits.

4.1.1 Energy Flexibility Models

Energy flexibility models for HVAC and EV have been used in previous research (Sundstrom & Binding, 2012), (Bessler S. D., 2015) to allow for flexible consumption between dynamically calculated low and high energy profiles.

4.1.1.1 HVAC

HVAC is used in Europe and US mainly for cooling (space heating uses natural gas). A standard thermodynamic model with thermostat control is used, in which losses through windows and walls, and heat gains from sun and the presence of people are considered. The HVAC cooling flexibility is illustrated in
Figure 4-2: HVAC flexibility example at t=0: the maximum consumption curve becomes flat when the minimum indoor temperature is reached. However, the room heats up via the walls and windows, so it eventually starts cooling again. If no cooling is done for a while, the maximum indoor temperature is hit, therefore cooling must be activated (see the Eflexmin curve in
Figure 4-2.

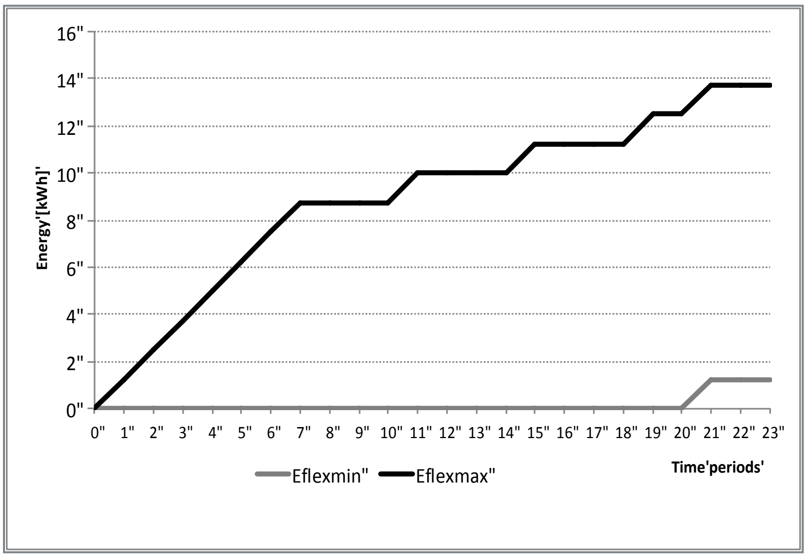

Figure 4-2: HVAC flexibility example at t=0

When apartment blocks or offices with many rooms are modeled, a tradeoff has to be made between the complexity encountered when modeling thermodynamically individual rooms (Chen), (Moroșan, 2010) and the need to have a simplified system that scales up with the number of buildings. The selected approach has been to use the total volume of the building, but to cool this "room" in many power intensity steps, instead of a single ON-OFF control. Finally, a calibration operation is needed to match the measured consumption data (available from the EIA open data) and the model consumption.
The advantage of the simplified model is that a single CEMS controller can be used for a shopping center, hospital or office building, such that the consumption for cooling, warm water, EV charging, or even PV generation can be aggregated.

4.1.1.2 Electric vehicle (EV)

Electric vehicle charging is modelled by tasks in which the EV has to be charged within a certain time interval with a given energy amount. The charging power is variable, but limited to maximum value.

EV charging can be performed with variable charging power. In Figure 4-3 the flexibility as calculated at current time t=0 is the cumulative charging energy. We observe that the EV has to be charged at time t=7 when it is supposed to leave. Therefore it has to start charging at latest t=3.

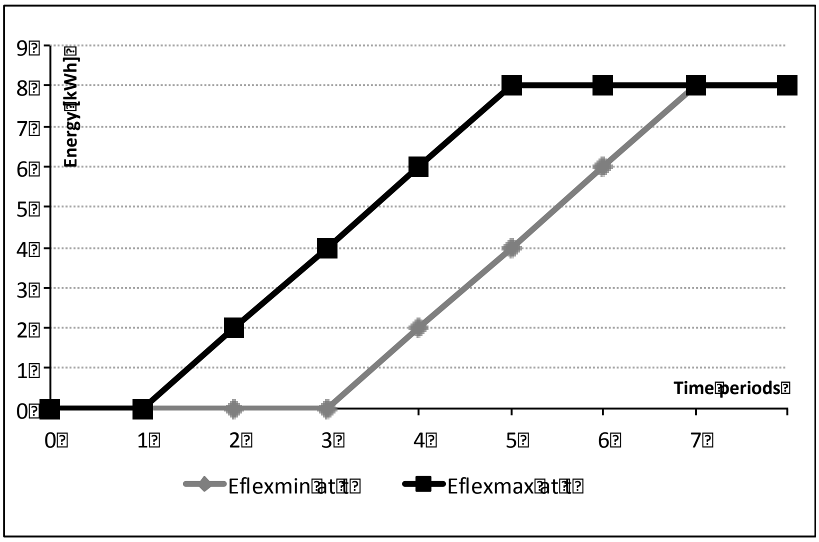

Figure 4-3: EV Charging flexibility at time t=0, before car arrives at t=1. Minimum and maximum demand are in this example both 8 kWh.

4.1.1.3 Electric Storage (ESS)

The ESS (energy storage system) model is similar to the EV, it provides maximum charging and discharging power values, and empty/full energy levels. In addition, a cyclic charge-discharge behavior is imposed by requiring that a minimum amount of energy to be reached once a day. The flexibility envelopes are depicted in Figure 4-4.

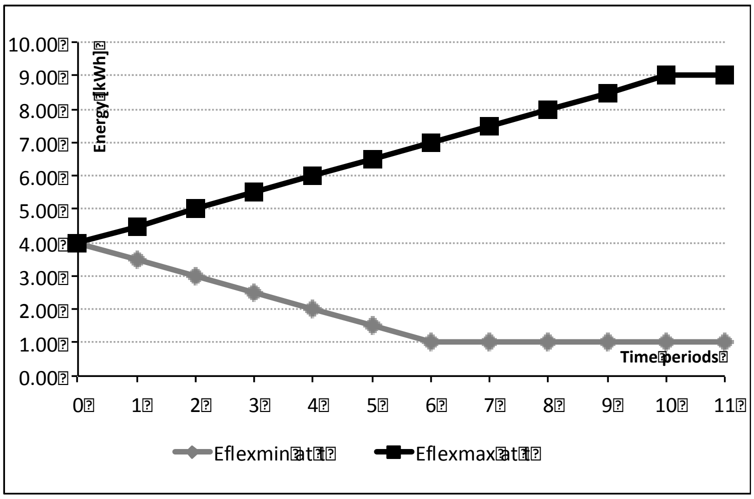

Figure 4-4: Battery storage flexibility, SOC=4 at t=0, discharge and charge rates 2kW, SOCmax =9, SOCmin=1kWh.

4.2 THE POWER OUTAGE MODE

In case an outage event is detected, the MG and CEMS controllers switch to outage mode. Following changes occur in the control system:

- the price dependent term is removed from the objective function, the load profiles still follow the setpoints and keep the strict balance between supply and demand, as mentioned in (Lopes, 2009)
- islanding policy rules are activated, see below.

In the real system the dispatchable local generation ramps up to keep the balance with the demand, however for the planning purpose we are mainly interested in how large this demand will be over the outage period, for different scenarios.

We assume that the communication infrastructure remains functional and the CEMS controllers are notified in case an outage occurs somewhere in the grid. As mentioned before, an outage event leads to one of the scenarios: islanding or power supply reduction. In case of islanding, the supplied energy by dispatchable generation is given and is used as input parameter by the MG controller. The load profiles still follow the setpoints and keep the strict balance between supply and demand, similarly to the description in (Lopes, 2009).
The "smartness" of a microgrid could materialize in a number of rules that are activated, once the outage event is received by the controllers in the microgrid. The rules can be more restrictive or more relaxed, depending on the energy balance, i.e. the amount of dispatchable generation available and the societal needs in the different building types. In the following we list a number of rules for the outage mode, that we have experimented with:

- Shedding the PV generation is not allowed, the PV output is maximized.
- The price dependent charging of the batteries is disabled; instead, the charging/discharging regime is controlled by "costs" determined by the PV availability (high PV generation means charging is recommended)
- the interruptible load is disconnected
- the air conditioning/heating may be switched off in certain buildings to save energy. In any case thermostat limits are relaxed to increase flexibility.
- EV charging is either disabled or may use only local renewable energy.

4.3 USED DATA SOURCES AND MODEL CALIBRATION

Grid characteristics: The low voltage grid has mostly a simple, radial topology. The full knowledge of the cable characteristics and lengths would allow a power flow calculation and imposing additional current and voltage limitations during the optimization. However, there is a practical drawback to this approach: the topology information at the LV grid level is known, if at all, only by the DSO. Therefore, since it is unlikely that city planers that would use this tool to get this information, we use simple power limits at the feeders and/or the secondary substation.

Energy prices: We use day-ahead market clearing prices in order to optimize the battery charging and discharging cycle. Although prosumers are allowed to inject power from excessive generation into the grid, to monetary function is currently used. The focus is on maximizing the usage of own produced energy.

PV generation: The solar irradiance data for the whole year in the Vienna region has been obtained. This data is dependent on the outside temperature, is a combination of direct and diffuse irradiation.

The efficiency factor η and the area A of the panels are also needed in order to calculate the power output of the panel. The rating effect of the inverter can also be considered, however we use the control variable gf to reduce the generated power, see (SolarGIS, kein Datum):

$$P_{max} = I_r \, \eta \, A$$

$$\eta = 16\%, \text{ for } P_{max} = 5\text{kW we need for instance } A = 32\text{m}^2$$

The model for PV power optimization has to reflect the business model. In case of one household with PV generation on the own roof, net metering can be applied in the sense that the consumption is compensated through the PV generation.

However for apartment buildings or other buildings with several tenants, more complex models are required, such as community share project or third party ownership. In a community shared project, each apartment owner receives compensation for an appropriate share of the produced power (using virtual net metering).

4.4 LOAD CHARACTERIZATION

A classification of loads in the context of emergency demand management has to be made. The reason for doing this is to act proactively, similarly to the “Emergency Demand Response” in which certain loads, known in advance are shed. However we do not discuss the monetary compensation involved in EDR.

In theory, it is simple to define the behaviour of a load in emergency case:

- **Critical load**: should not be interrupted, load should be met. In this category we should include

  - partial lighting in houses, commercial places, industrial
  - local controllers (e.g. CEMS), microgrid controller
  - wireline communications (ICT infrastructure for control, internet), WLAN, cellular nodes and antennas, ATM power and communication (not clear if possible because it implies banking infrastructure has to work as well).
  - refrigerators in food stores, pharmacies, hospitals, storage houses.
  - water pump for district/town
  - gasoline pumps in gas stations
  - lifts and automatic doors in house blocks and commercial
  - special critical infrastructures to be discussed separately: hospital, pharmacy
  - apartment gas and water heating, (because of the electronics).

- **Interruptible load is** disconnected in an outage case. The realization of interruptible loads will help to save money when dimensioning the local power generation capability. Examples of interruptible loads in the household: high loads in the kitchen, entertainment, washing machine, vacuum cleaner, etc.

A third possibility is to reduce the load, or to shift it in time, without having to interrupt it completely. The amount of the reduction results from a flexibility model. Depending on the individual scenario, type of building, etc. a flexible load can be also completely interrupted. Examples of flexible loads used in our model are:

- Electric house heating/air conditioning: has on/off control for each of the defined zones of the house or building. In outage/emergency situations the HVAC is switched off and the temperature limits are relaxed to increase energy flexibility.

- EV charging, is flexible, the minimum charged energy is curtailed in case the supplied energy is not sufficient.

- Home battery storage: its charging/discharging operation will not be interrupted in outage case.

4.4.1 Using the consumption data

Other than in Section 3.2, the consumption profiles obtained here are for the whole year at an hourly resolution. More important for the further processing is the fact that the consumption is de-aggregated according to defined categories. The categories found in the data (EIA, 2012) are: ventilation, cooling, heating, lights and equipment. Further, it is necessary to define which part of the consumption is to be defined as critical or interruptible.

In case of the supermarket, there is a large power amount attributed to refrigeration which is critical. The thermodynamic model has to be calibrated for the size of the building. Thus, the air flow cooling and heating can be considered as flexible loads (should fit the data). The lights and equipment are in case of commercial buildings critical loads.

In the IEA dataset and also throughout Europe, (depending on building type and climate region), heating and water heating is often done with natural gas. Therefore, the visible electricity consumption during the summer due to air conditioning is higher than in winter.

4.5 THE CEMS MODELS USED FOR DIFFERENT BUILDING TYPES

The basic data has been taken from EIA (EIA, 2012) where we selected Chicago as the climatic region close to that of Europe. The thermostat limits were set to [22-25]°C and we focused on the summer months, where cooling is done electrically (air conditioning).

Building type	Size [m^2],	HVAC zones	Critical	Interruptible	Add ons
Residential apartment building	3100	30	Fan, ICT equipment, lights	HVAC, facility	
Small office	511	8	Fan, ICT equipment, lights	HVAC	PV 8 kWp
Residential house	250	4	Lights, ICT equipment, fan	EV HVAC	PV 4kWp
Supermarket	4180	20	Refrigeration, lights, ICT equipmenent		
Outpatient clinic	3804	50	Fa, ICT, lights, HVAC		
Battery	0	0	Batt. 100kW		

Table 1 Summary of Building charcteristics

4.5.1 Residential apartment building

Model calibration: Consumption on 2th and 3th of July according to EIA data: 345kWh in 48 h. The calibration is achieved introducing the coolingFactor parameter, such that the Consumption of the model is 341 kWh in 48h is the same as in the EIA data.

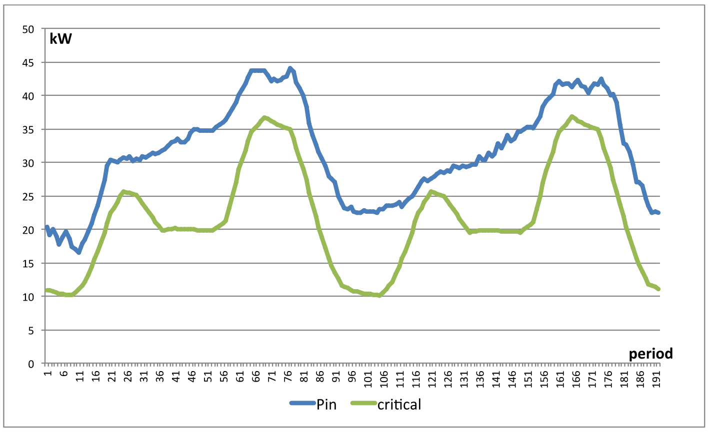

Figure 4-5: *Apartment building*: actual consumption (including flexible and interruptible), critical demand.

4.5.2 Residential House

Model calibration: Consumption in July according to EIA is between 3 to 5kWh per 24h. With a coolingFactor=10, we get from the simulation a consumption of 4 kWh day.

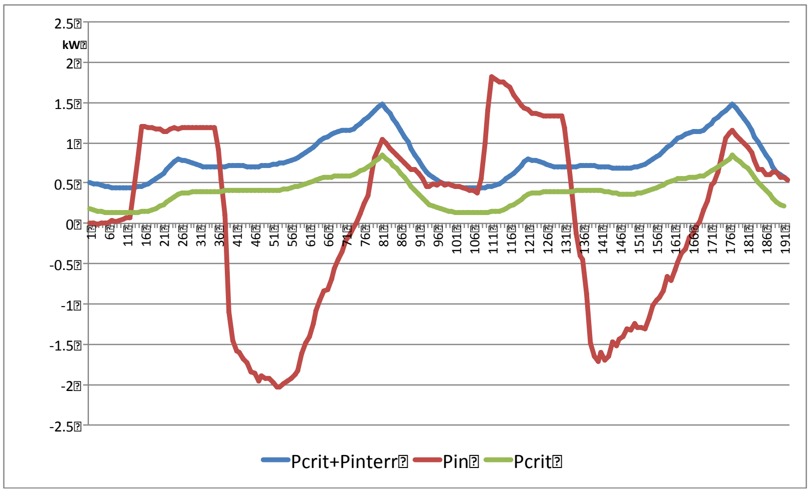

Figure 4-6: *Residential house*: House net power flow P_{in}, critical load P_{crit} and interruptible load P_{interr}, 48 hour profile.

4.5.3 Small Office

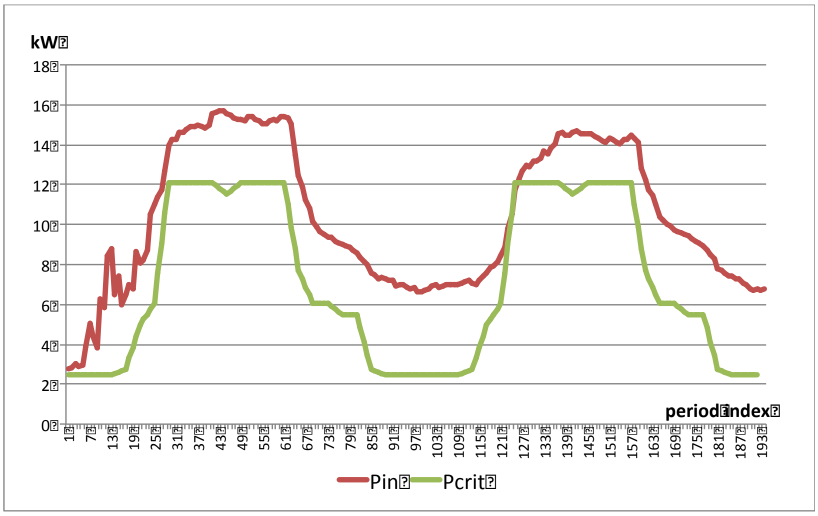

Figure 4-7: Small office*:* net power flow P_{in}, critical loads, no PV generation

4.6 MODELS FOR DEMAND OPTIMIZATION

4.6.1 CEMS Optimization

Optimization problem formulation

Notation	Description
C	connected flag, false if outage mode
x_j	battery charging (> 0) or discharging (< 0) power
y_j	charging power in kW during period j
z_j	HVAC cooling control during period j
gf_j	generation factor during period j
E_j^{EV}	EV charged energy starting with j=0
E_j^{HVAC}	energy consumed for cooling
P_{max}^{EV}	maximum EV charging power
E_j^{ESS}	energy stored in the battery
P_j^{crit}	critical load active power during period j
P_j^{interr}	interruptible load active power during period j
P_j^{gen}	nominal PV generated power in period j
c_j	MCP energy price during period j
P_j^{ref}	setpoint imposed on the CEMS in period j
LV_{maxp}	limiting power constraint for the whole grid

Table 2: Notation Summary

The energy management system EMS is a local controller that servers a household or a whole building. In a microgrid, the energy price for the customers is determined by the market price and by the local generation. An end user could use the daily market price variations for battery charging/discharging operations. (K3 term in the objective (5) below)

In each time interval we solve a MIP optimization problem, using the MPC scheme. For more details, see (Bessler S. D., 2015) and (Bessler S. J., 2016). In the normal, non-islanded mode (flag C=1), the CEMS objective function has the terms, as in objective (5):

- follow the setpoints received from the MG controller,
- maximize the generated PV active power gf_j $P^{gen}{}_j$ and
- maximize the profit by charging the battery when the energy price is low.

In normal operation mode we define following rules:

- both critical and interruptible loads are served
- EV, HVAC and battery operate and the HVAC flexibility relates to the user defined indoor temperature range.
- PV power injection into the grid is allowed.

minimize

$$K_1 \sum_{j \in N} (P_j^{in} - P_j^{ref})^2 - K_2 \sum_{j \in N} gf_j P_j^{gen} + K_3 \sum_{j \in N} c_j x_j \quad (5)$$

subject to:

$$P_j^{in} + gf_j P_j^{gen} - y_j - x_j - P_j^{crit} - C(P_j^{interr} + z_j P^{HVAC}) = 0, j \in \quad (6)$$

$$E_j^{EV} = E_{j-1}^{EV} + y_{j-1} T, j \in N - \{0\}, E_0^{EV} = 0 \quad (7)$$

$$E_j^{EV} \in [\underline{E}_j^{EV}, \overline{E}_j^{EV}], j \in N \quad (8)$$

$$E_j^{HVAC} = E_{j-1}^{HVAC} + z_j P^{HVAC} T, j \in N - \{0\}, \quad (9)$$

$$E_0^{HVAC} = z_0 P^{HVAC} T \quad (10)$$

$$E_j^{HVAC} \in [\underline{E}_j^{HVAC}, \overline{E}_j^{HVAC}], j \in N \quad (11)$$

$$y_j \in [0, P_{max}^{EV}], j \in N \quad (12)$$

$$z_j \in \{0, zones_j\}, j \in N \quad (13)$$

$$gf_j \in [gf_{min}, 1], j \in N \quad (14)$$

$$x_j \in [-P_{dis}^{ESS}, P_{chg}^{ESS}], j \in N \quad (15)$$

$$E_{j+1}^{ESS} - E_j^{ESS} - \eta x_j T = 0, j \in N - \{0\}, E_0^{ESS} = 0 \quad (16)$$

$$E_j^{ESS} \geq \underline{E}_j^{ESS} = \max(E_0^{ESS} - jP_{dchrg}^{ESS}/T, E_{min}^{ESS}) j \in N \quad (17)$$

$$E_j^{ESS} \leq \overline{E}_j^{ESS} = \min(E_0^{ESS} + jP_{chrg}^{ESS}/T, E_{max}^{ESS}) j \in N \quad (18)$$

$$E_0^{ESS} = E0 \quad (19)$$

$$E_{j=mod(N)}^{ESS} \geq E0 \quad (20)$$

Equation (6) expresses the consumption generation power balance. Equations (7), (10) and (16) express the energy changes in EV, HVAC and the battery, whereas (8), (11) and (17) require that the energy is within the flexibility limits. The local control signals are described by constraints (7), (8) and (10). The results of the computation are:

- predicted active power consumption P^{in}_j of the building associated to that CEMS (respectively power injection into the grid if the values are negative).
- predicted control actions: a) HVAC control z_j, b) EV charging intensity y_j c) PV inverter output shedding gf_j, d) ESS charging/discharging power x_j.

4.6.2 The MG controller

The microgrid controller is bidirectionally connected with CEMS controllers or DER nodes in the LV grid. Tasks related to the energy price fixing in interactions with the energy market and the local generators are not discussed in this work. We focus on the demand management functionality: the MG is aware of the maximum power that can be drawn from the grid in normal mode or outage mode, including the local generation. In the same way, it keeps the injected power into the grid below the allowed limit. A simple optimization model computes the setpoint profile to be sent to each CEMS.

In the outage case (C=false), the total power is limited to the maximum locally generated power LV°_{maxp} instead to LV_{maxp} and has to supply the remaining critical and flexible loads. Inequalities (23) and (24) make sure that the setpoints $P_i^{in}+ß_i$ are within the flexibility limits of the CEMS.

$$\alpha \sum_{i \in B} \beta_i^2 + (1-\alpha) \sum_{i \in B} (P_i^{in} + \beta_i - P_i^{ref-})^2; \alpha \in [0,1] \quad (21)$$

subject to:

$$\sum_{i \in B} (P_i^{in} + \beta_i) \leq C \cdot LV_{maxp} + (1-C) LV^o_{maxp} \quad (22)$$

$$\beta_i \leq \overline{E}_i^{CEMS}/T - \sum_{k \in N | k \leq j} P_{ki}^{in}, i \in B \quad (23)$$

$$\beta_i \geq \underline{E}_i^{CEMS}/T - \sum_{k \in N | k \leq j} P_{ki}^{in}, i \in B \quad (24)$$

The microgrid simulation realizes a control loop between the MG controller and the buildings CEMS controllers. As long as the maximum admissible load or injection power in the grid is not exceeded, the building components receive the demand they ask for. Setpoints are sent every 15 minutes to the building components. The flexible loads, PV generation and battery are operating in normal conditions. At a previously defined point in time the outage event is received by both MG and CEMS controllers, the interruptible loads are lost and emergency rules are triggered. The consumption goes down. If LV°_{maxp} has been previously defined, it will not be exceeded by the loads. Following the simulation results dispatchable generation can be dimensioned depending of the outage scenario (islanding or reduced power supply).

4.7 SIMULATION RESULTS

4.7.1 An Evaluation Metric

The behaviour of the grid in extreme situations, natural calamities or cyber attacks is usually characterized by a resilience metric (Mancarella, 2015), (Sandia National Laboratories, 2015), see also the references in Section 3.5.

This measure covers all the phases of the outage, including the restoration of the grid state and the repair of damaged equipment. If parts of the grid continue to operate as islands, the resilience of the whole grid increases.

In order to assess the quality of an outage response with the mechanisms we have described in the previous sections, we are searching for a more specific metric that can be computed following the simulations.

We consider therefore the energy E^{o}_{in} that still has to be supplied to the microgrid during an outage. The demand of the microgrid during normal operation D^n is the sum of critical, interruptible demand, whereas the energy difference in the storage at the end of the considered interval ESS^n_{diff}

$$D^n = E_{crit} + E_{interr} + ESS^n_{diff}$$

The demand D^n has to be satisfied by the renewable generation E_{RES} and the power injected into the microgrid E^n_{in}

$$D^n = E^n_{in} + E_{RES}$$

Similarly, in outage mode $D^o = E_{crit} + ESS_{diff}^o$ and $D^o = E^o_{in} + E_{RES}$

Lets define the autonomy factor

$$\alpha = 1 - \frac{E^o_{in}}{D^n} = 1 - \frac{E^o_{in}}{E^n_{in} + E_{RES}} \quad (17)$$

Using the definitions above, we obtain $\alpha = \frac{E_{interr} + (ESS^n_{diff} - ESS^o_{diff}) + E_{RES}}{E_{crit} + E_{interr} + ESS^n_{diff}}$

For a non-smart grid where all the loads are considered critical, $E_{interr}=0$, no renewable $E_{RES}=0$, $\alpha \approx 0$. Increasing E_{RES} can theoretically achieve a self sufficient microgrid. In reality the renewable power fluctuates strongly, therefore dispatchable generation must be used.

In our experiments, the terms in expression (17) can be measured, therefore the autonomy factor will be calculated.

4.7.2 Simulation Setup and preliminary runs

A random configuration of buildings consisting of 8 offices, 4 midrise apartment blocks and 26 residential houses has been simulated for a duration of two days. Outages of different durations such 6, 12, 24 hours have been simulated, starting in the second day at 9am. The Power limitations at the transformer of 300kW and 200 kW for the outage, were set high enough not to constrain the power allocation for these tests.

A typical simulation is shown in

Figure 4-8: after 36 hours of normal operation, an outage of 24 hours leads to a sharp drop in the consumption.

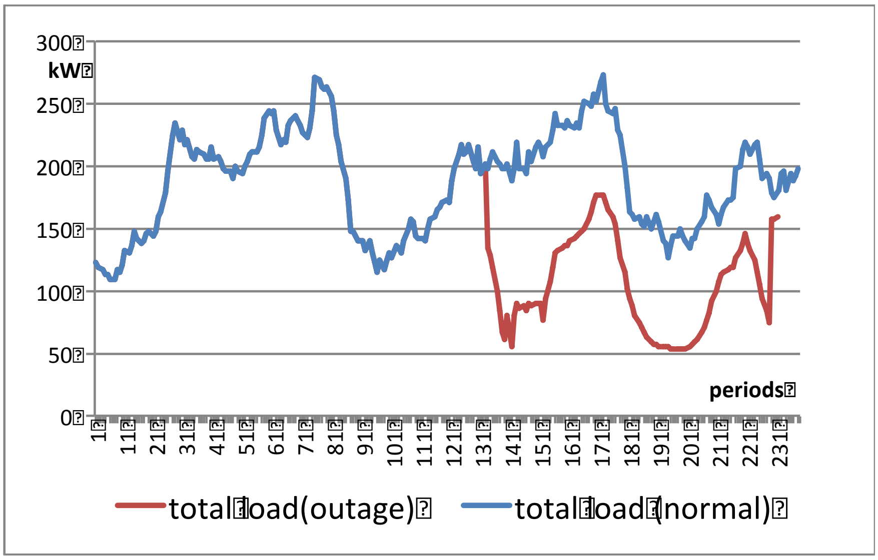

Figure 4-8: Microgrid net consumption, normal and 24h outage simulations.

A series of experiments have been conducted to evaluate the impact of different system parameters on the proposed grid autonomy factor. Thus, we varied the outage duration, the amount of renewable generation and battery storage in the microgrid.
We start with a scenario (see Table 3) we denote the *baseline* scenario, in which the outage duration is 24 hours, each small office has 50m^2 PV panels, and each residential house has a 10kWh battery. The other scenarios are compared to this baseline:

- NoPV: the offices have no PV generation
- LessStorage: each residential house has only 5kWh battery.
- 6hOutage: the outage duration is 6 hours instead of 24h, from 9am to 3pm.
- 120kW: the demand during the outage should not exceed 120kW (was 200kW).

Scenario	E^n_{in} MWh	E^o_{in} MWh	E^n_{RES} MWh	α
Baseline	4.675	2.46	1.15	0.58
NoPV (offices)	5.11	2.90	0.71	0.50
LessStorage	4.77	2.40	1.04	0.58
6hOutage	1.23	0.55	0.47	0.67
24hOutage-120kW	4.675	2.39	1.15	0.54
6hOutage-120kW	1.23	0.59	0.47	0.65

Table 3: Impact of the system parameters on the autonomy factor

More PV generation clearly improves the autonomy factor (see the difference between the scenario NoPV, and the baseline.

One would expect that the increase of the battery storage in the grid would increase the autonomy factor. Surprinsingly, the latter does not change. The reason is that both for smaller and larger batteries, the charging and discharging due to PV generation makes no difference in the net consumption (see Figure 4-9). An eventual PV power surplus from a certain household is immediately consumed by other buildings that have a net demand. Therefore, the net energy needed by the microgrid during the outage does not change with the storage capacity. A completely different situation is of course when an outage can be met prepared, with full batteries.

The outage duration and its timing do influence the autonomy factor: thus, an outage of only 6h (9am to 3pm) increases α from 0.58 (the value for 24h) to 0.67.

Finally, we went to test the use of the Demand Management capability to limit the load during the outage: this feature is needed after a certain amount of dispatchable generation has been installed. In preliminary simulations, the power constraint has been set to 120kW (was previously 200kW), leading to an expected decrease of α see Table 3.

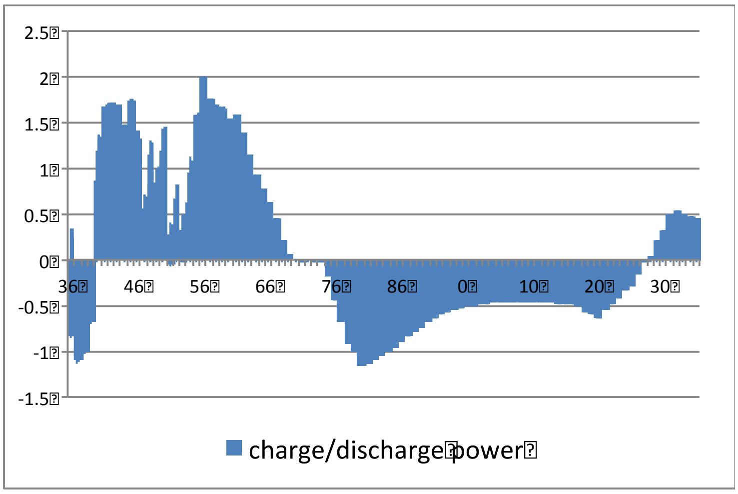

Figure 4-9: Battery charging/discharging regime during the outage

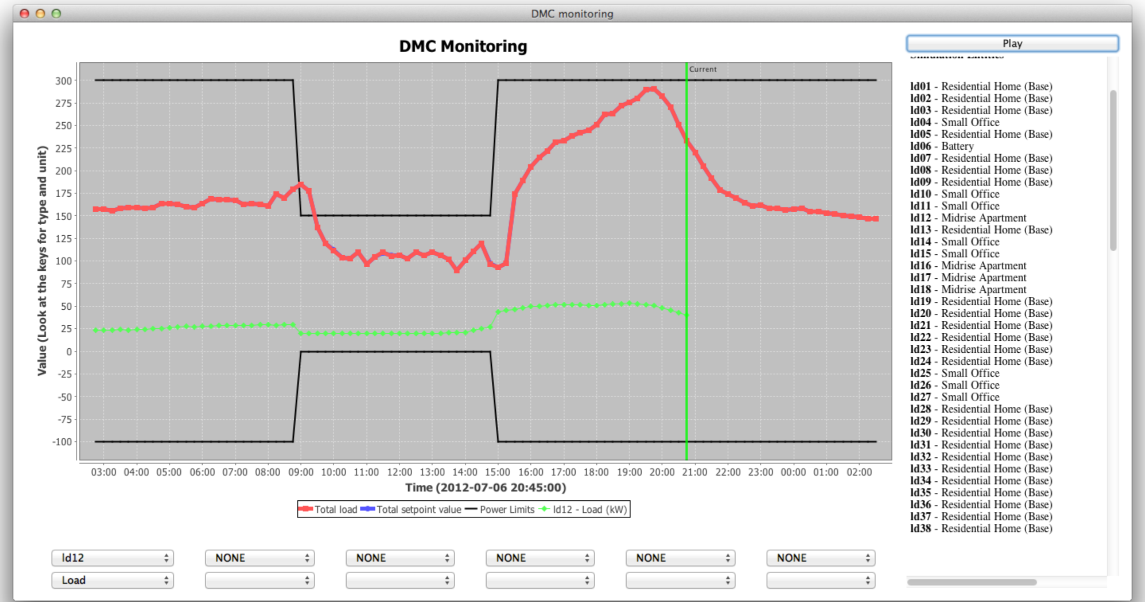

Figure 4-10: Graphical output of the simulation tool: total consumption of the grid (list on the right) in the past and in the prediction horizon (right of the current time vertical green line). Black line: MG consumption limits normal/outage mode.

5 SUMMARY AND CONCLUSIONS

In this Deliverable we have developed models for the characterization of consumption data, as well as the architectural basis to develop tools for the evaluation the effect of outages in different levels of the grid. In a mid-voltage, general grid topology we handle outages that lead to topology changes, individual link and node (generation) failures, etc., whereas at the microgrid level, we do not handle individual node or link failures, but use flexible loads and demand management mechanisms for a “soft” degradation of service.

The major contributions are listed below:

The **demand profiling** is achieved in Section 3.2 using the available diurnal demand data in the public domain. The average daily profile for a particular groups of consumers are selected and to be further stitched together with the annual demand trend that forms the annual trend of energy demand. The state representation of electrical signal is used as the profiling equation to the microgrid model. The profiled annual demand provides the realistic estimations. As there are available demand data in the public domain, this has also added the flexibility and simplicity in modelling the overall energy demand with only a few parameters.

The resultant demand profile is further applied in the active-aware-based **EnKF field for demand forecast** and assimilation. The EnKF evaluation results demonstrate the capability and robustness of EnKF in forecast and matching the energy demand, either in real-time or based on prior knowledge and historical records. However, as EnKF is a Monte Carlo type of data assimilation, the low EnKF realisation will result in poor forecast. The realisation of $N_e = 500$ in this example provides the sufficient convergence of EnKF propagations. For this reason, EnKF allows the convergence of data assimilations, in the condition that that the ensemble size selected is sufficiently large. Additionally, the nonlinearity in different profiles of consumers will arise and therefore the identification of state variables, initial conditions and prior knowledge of the EnKF model are therefore necessary in order to provide the better demand forecast with minimised EnKF propagation errors.

In the lower microgrid level, the **demand profiling** in Section 4.5 needs the critical and interruptible components in order to feed the demand management mechanisms.

The **optimisation** model in Section 3.4 allows the whole integration of the main grid supply, electricity connections, distributed generations (e.g. wind, PV, backup generators), storage systems, energy demand profiles (large loads, substations, hospital), and the perturbation of power outages (due to disasters, terrorist attacks, grid failures). The **contingency simulation** is also considered in the model, where scenarios of power outage due to disasters or any other valid circumstances can be simulated. In this model, the *N*-1 contingency criterion is applied.
Al the microgrid level, a **demand management** scheme realized in a central and building (CEMS) controllers is proposed in Section 4.6.

In both frameworks simulation **experiments** for normal and outage mode operation are performed and the results are evaluated based on similar criteria: resilience respectively autonomy factor in the microgrid setting.

The results in Section 3.6 show the behaviour of generators in case of N-1 contingency or islanding, as well as the storage operations.

At the microgrid level, the simulation experiments in Section 4.7.2 quantify a) the impact of outage duration on the resilience (autonomy factor), b) the important influence of the amount of renewable energy on the autonomy factor and c) the impact of the limited power of local dispatchable generation on the autonomy factor. It is also explained the negligible effect of different amounts of battery storage on the outage response performance.

The summary of cost savings associated to the business-as-usual and optimised solution corresponding to different scenarios are shown in Table 5-1.

Scenario	Description	Cost savings (£)
1	Normal grid-connected operation and economic islanding	1724.30
2	Islanded operation due to the failure of one power generation node	1850.80
3	Islanded operation due to the outage in the mid-level grid	5007.28

Table 5-1 Cost savings of operation associated to business-as-usual and optimised solution corresponding to different scenarios

Based on Table 5-1, good saving is achieved in Scenario 1 where the economic islanding is employed that avoids the purchase of high-electricity price from the main grid. Thus the concept of economic islanding provides a valuable contribution of negligible grid costs during the peak periods. In contrast, the amount of cost saving Scenario 2 is higher than Scenario 1 due to the failing operable state in one of the generators with the high cost of operation. However, as it is highly uncertain in the operable state (operational or non-operational due to failure) of corresponding generators, the amount of savings achieved in Scenarios 1 and 2 are uncorrelated. It is not the scope of this report to compare the effectiveness of cost savings in each scenario due to different operational and islanding purposes. In Scenario 3, the huge amount of saving achieved shows the positive aspects of the grid in isolating the operation during the mid-level grid outage. Even though the huge amount of saving is achieved in Scenario 3, it should be noted that the continuous isolation of mid-level grid with other parts of microgrids may breach or worsen the required margin for stability and security of electricity supply. Henceforth, the penetration of islanded operation must be maintained regularly.

The presented models are at the basis of the planning tools developed in WP4.

6 REFERENCES

Almendral-Vazquez, A., & Syversveen, A. R. (2006). Ensemble Kalman Filter - Theory and Applications in Oil Industry. *NR Publication, NR-notat SAND/05/06*, pp. 1-25.

Anderson, J. (2012, July). Localization and Sampling Error Correction in Ensemble Kalman Filter Data Assimilation. *Americal Meteorological Society, 140*, pp. 2359-2371.

APX Power Spot Exchange. (2016a). *Profile*. Retrieved from APX: http://www.apxgroup.com

APX Power Spot Exchange. (2016b). *UKPX RPD Historical Data*. Retrieved from APX: https://www.apxgroup.com/market-results/apx-power-uk/ukpx-rpd-historical-data/

Bahramirad, S. (2012). Economic and Emergency Operations of The Storage Systems in a Microgrid. *Degree Dissertation, Electrical Power Systems Second Level*. Stockholm, Sweden: KTH Royal Institute of Technology.

Barklund, E. P.-A. (2008). *Energy management in autonomous microgrid using stability-constrained droop control of inverters.* Power Electronics, IEEE Transactions on, 23(5), 2346-2352.: IEEE.

Bessler, S. D. (2015). Using flexibility information for planning the energy demand of households. *Communications in Computers and Information science, vol. 579, pp 216-236, ISBN 978-3-319-27752-3, Springer 2015*.

Bessler, S. J. (2016). Energy Management in Microgrids with Flexible and Interruptible Loads. *Innovative Smart Grid Technologies (ISGT).* Minneapolis: IEEE.

Bollinger, L. A. (2015). Fostering Climate Resilient Electricity Infrastructure. Delft: Delft University of Technology.

Cano-Andrade, S., von Spakovsky, M. R., Fuentes, A., Lo Prete, C., Hobbs, B. F., & Mili, L. (2012). Multi-objective Optimization for The Sustainable-Resilient Synthesis/Design/Operation of a Power Network Coupled to Distributed Network Producers via Microgrids. *Energy, vol. 6, Part A and B*, pp. 1393-1408.

Chen, C. W. (n.d.). MPC-based appliance scheduling for residential building energy management controller. *IEEE Transactions on Smart Grid, 4(3), 1401-1410.*

DECC. (2014). *Sub-National Electricity and Gas Consumption Statistics: Analysis Tool 2005 to 2014*. Retrieved from Department of Energy and Climate Change: https://www:gov:uk/government/publications/sub-national-electricityand-gas-consumption-statistics-analysis-tool-2005-to-2009

Dike, D. O., & Mahajan, S. M. (2008). Utilization of L-index in Microgrid Interconnected Power System Network. *2008 IEEE Power and Energy Society General Meeting - Conversion and Deliver of Electrical Energy in the 21st Century*, pp. 1-8.

DNV GL. (2014). *Microgrid Optimizaer - A Holistic Operational Simulation Tool to Maximize Economic Value or Electric Power Reliability.* Retrieved from DNV GL:

http://production.presstogo.com/fileroot7/gallery/DNVGL/files/original/3a1dd794f6ff46b9a279175c15af0f11.pdf

DoE. (2011). *Module 5: Energy Assessment - Demand Analysis.* Retrieved from Department of Energy Republic of South Africa: http://www.energy.gov.za/EEE/Projects/Building%20Energy%20Audit%20Training/Training%20Modules/Building%20Energy%20Auditing%20Module%205_final.pdf

EIA. (2012). *Energy Information Administration (US)*. Retrieved from http://www.eia.gov/consumption/commercial/data/2012/

Elexon. (2013). *Load Profiles and Their Use in Electricity Settlement.* Retrieved from Elexon: https://www.elexon.co.uk/wp-content/uploads/2013/11/load_profiles_v2.0_cgi.pdf

Elexon. (2016). *What is Load Profile?* Retrieved from Elexon: https://www.elexon.co.uk/reference/technical-operations/profiling/

Evensen, G. (1994, May). Sequential Data Assimilation with a Nonlinear Quasi-Geostrophic Model Using Monte-Carlo Methods to Forecast Error Statistics. *Geophysical Research, col. 99, no. 5*, pp. 10143-10162.

Evensen, G. (2003, November). The Ensemble Kalman Filter: Theoretical Formulation and Practical Implementation. *Occean Dynamics, vol. 53, no. 4*, pp. 343-367.

Flath, C., Nicolay, D., Conte, T., van Dinther, C., & Filipova-Neumann, L. (2012). Cluster Analysis of Smart Metering Data - An Implementation in Practice. *Business & Information Systems Engineering, 4*, pp. 31-39.

Gillijins, S., Mendoza, O. B., Chandrasekar, J., De Moor, B. L., Berstein, D. S., & Ridley, A. (2006). What is Ensemble Kalman Filter and How Well Does it Work? *2006 Americal Control Conference* (pp. 4448-4453). Minneapolis, MN: IEEE, DOI: 10.1109/ACC.2006.1657419.

Gurobi. ( ). *Gurobi Solver*. Retrieved June 1, 2016, from http://www.gurobi.com/.

Hedman, K. W., Ferris, M. C., O'Neill, R. P., Fisher, E. B., & Oren, S. S. (2010, May). Co-Optimization of Generation Unit Commitment and Transmission Switching with N-1 Reliability. *IEEE Transactions on Power Systems, vol. 25, no. 2*, pp. 1052-1063.

Huang, H., & Zhuang, W. (2014, March). Stochastic Modelling and Optimization in a Microgrid: a Survey. *Energies, vol. 7, no. 4*, pp. 2027-2050.

Jayaweera, D., & Islam, S. (2014, April). Security of Supply in Active Distribution Networks with PHEV-based Strategic Microgrids. *Parts of The Series Reliable and Sustainable Electric Power and Energy Systems Management, DOI: 10.1007/978-81-322-1798-5_2*, pp. 17-31.

Jensen, J. P. (2007). Ensemble Kalman Filtering for State and Parameter Estimation on a Reservoir Model. *Master Thesis, Department of Engineering Cybernetics*. Trondheim, Norway: Norwegian University of Science and Technology.

John, C. J., & Mandel, J. (2008, March). A Two-Stage Ensemble Kalman FIlter for Smooth Data Assimilation. *Environmental and Ecological Statistics, 15*, pp. 101-110.

Katiraei, F. I. (2005). Microgrid autonomous operation during and subsequent to islanding process. *IEEE Transactions on power delivery, 20(1), 248-257.* .

Khodaei, A. (2014a, May). Microgrid Optimal Scheduling with Multi-Period Islanding Constraints. *IEEE Transactions on Power Systems, vol. 29, no. 3,* pp. 1383-1392.

Khodaei, A. (2014b, July). Resiliency-Oriented Microgrid Optimal Scheduling. *IEEE Transactions on Smart Grid, vol. 5 no. 4*, pp. 1584-1591.

Lau, E. T. (2016). Quantification of Carbon Emissions and Savings in Smart Grids. *PhD Thesis, College of Engineering, Design and Physical Sciences*. Uxbridge, Middlesex, UK: Brunel University London.

Lau, E. T., Yang, Q., Forbes, A. B., Wright, P. S., & Livina, V. N. (2014, April). Modelling Carbon Emissions in Electrical Systems. *Energy Conversion and Management, 80*, pp. 573-581.

Lopes, J. A. (2009). *Advanced Architectures and Control Concepts for More Microgrids.* Deliverable of STREP Project "More Microgrids".

Mancarella, M. P. (2015). The Grid: Stronger, Bigger, Smarter? Presenting a Conceptual Framework of Power System Resilience. *IEEE Power and Energy Magazine, vol. 13, no. 3, pp. 58-66, May-June 2015.* .

McLoughlin, F., Duffy, A., & Conlon, M. (2015, March). A Clustering Approach to Domestic Electricity Load Profile Characterisation Using Smart Meter Data. *Applied Energy, 141, DOI: 10.1016/j.apenergy.2014.12.039,* pp. 190-199.

Moroşan, P. D. (2010). Building temperature regulation using a distributed model predictive control. *Energy and Buildings, 42(9), 1445-1452.* .

NACHHALTIGwirtschaften. (n.d.). *Research & Implementation Building Blocks for The Active Distribution Grid*. Retrieved from NACHHALTIGwirtschaften: http://www.nachhaltigwirtschaften.at/(en)/publikationen/forschungsforum/131/teil2.html#h1

Naevdal, G., Johnsen, L. M., Aanonses, S. I., & Vefring, E. H. (2003). Reservoir Monitoring and Continuous Model Updating Using Ensemble Kalman Filter. *in SPE Annual Technical Conference and Exhibition* (pp. 1-12). Denver, Colorado, USA: SPE.

National Grid. (2016). *Data Explorer*. Retrieved from National Grid: http://www2:nationalgrid:com/UK/Industry-information/Electricity-transmission-operational-data/Data-Explorer/

NYSERDA, DPS, & DHSES. (2014). Microgrids for Critical Facility Resiliency in New York State. *Technical Report Number: 14 - 36*. New York.

Olivares, D. E.-S.-E. (2014). Trends in microgrid control. Smart Grid, IEEE Transactions on, 5(4), 1905-1919.

OpenEI. (n.d.). *Commercial and Residential Hourly Load Profiles for all TMY3 Locations in the United States*. Retrieved from OpenEI: http://en.openei.org/datasets/dataset/commercial-and-residential-hourly-load-profiles-for-all-tmy3-locations-in-the-united-states

Parisio, A. R. (2014, Sept.). A Model Predictive Control Approach to Microgrid Operation Optimization. *Control Systems Technology, IEEE Transactions on, vol.22*, (no.5,), pp. pp.1813-1827,.

Sandia National Laboratories. (2015). *Conceptual Framework for Developing Resilience Metrics for the Electricity, Oil, and Gas Sectors in the United States.* Sandia Report, 2015. SAND2014-18019.

Saravanan, B., Das, S., Sikir, S., & Kothari, D. P. (2013, April). A Solution to The Unit Commitment Problem - A Review. *Frontiers in Energy, vol. 7, no. 2*, pp. 223-236.

SolarGIS. (n.d.). *SolarGIS*. Retrieved from http://solargis.info/doc/solar-and-pv-data

Sundstrom, O., & Binding, C. (2012). Flexible Charging Optimization for Electric Vehicles Considering Distribution Grid Constraints. *IEEE Transactions on Smart Grid, vol.3, no.1, pp.26,37, March 2012.* .

Zendehdel, N., Karimpour, A., & Oloomi, M. (2008). Optimal Unit Commitment Using Equivalent Linear Minimum Up and Down Time Constraints? *2nd IEEE International Conferencec on Power and Energy (PECon 08)* (pp. 1021-1026). Johor Bahru, Malaysia: IEEE.

(Lopes, 2009) Lopes, J. A. P., Vasiljevska, J., Ferreira, R., Moreira, C., Madureira, A. (2009). Advanced Architectures and Control Concepts for More Microgrids.

(Parisio, 2014) Parisio, A., Rikos, E., & Glielmo, L. (2014). A model predictive control approach to microgrid operation optimization. *Control Systems Technology, IEEE Transactions on*, *22*(5), 1813-1827.

(Olivares, 2014)} Olivares, D. E., Mehrizi-Sani, A., Etemadi, A. H., Canizares, C., Iravani, R., Kazerani, M., ... , Jimenez-Estevez, G. (2014). Trends in microgrid control. Smart Grid, IEEE Transactions on, 5(4), 1905-1919.

(Bessler S. J., 2016) Bessler,S., Jung, O., Energy Management in Microgrids with Flexible and Interruptible Loads, Innovative Smart Grid Technologies (ISGT), 6-9 Sept. 2016, Minneapolis, US.

(Bessler S. D., 2015): Bessler, S., Drenjanac, D. , Hasenleithner E., Silva N., Using flexibility information for planning the energy demand of households, in Communications in Computers and Information science, vol. 579, pp 216-236, ISBN 978-3-319-27752-3, Springer 2015.

(SolarGIS, kein Datum)} SolarGIS, online: http://solargis.info/doc/solar-and-pv-data

(EIA, 2012) US Energy Information Administration, CBECS, online: http://www.eia.gov/consumption/commercial/data/2012/

(Sandia National Laboratories, 2015) Sandia National Laboratories, Conceptual Framework for Developing Resilience Metrics for the Electricity, Oil, and Gas Sectors in the United States, Sandia Report, 2015. SAND2014-18019.

(Katiraei, 2005) Katiraei, F., Iravani, M. R., \& Lehn, P. W. (2005). Microgrid autonomous operation during and subsequent to islanding process. IEEE Transactions on power delivery, 20(1), 248-257.

(Chen) Chen, C., Wang, J., Heo, Y., \& Kishore, S. (2013). MPC-based appliance scheduling for residential building energy management controller. IEEE Transactions on Smart Grid, 4(3), 1401-1410.

(Sundstrom & Binding, 2012), Sundstrom, O.; Binding, C., "Flexible Charging Optimization for Electric Vehicles Considering Distribution Grid Constraints," IEEE Transactions on Smart Grid, vol.3, no.1, pp.26,37, March 2012.

(Moroşan, 2010)Moroşan, P. D., Bourdais, R., Dumur, D., \& Buisson, J. (2010). Building temperature regulation using a distributed model predictive control. Energy and Buildings, 42(9), 1445-1452.

(Mancarella, 2015) M. Panteli and P. Mancarella, "The Grid: Stronger, Bigger, Smarter?: Presenting a Conceptual Framework of Power System Resilience," in IEEE Power and Energy Magazine, vol. 13, no. 3, pp. 58-66, May-June 2015.

(Gurobi,) Gurobi Solver, online: http://www.gurobi.com

A APPENDIX: CALCULATION OF THERMODYNAMIC COEFFICIENTS

.

We use the equation below

$$Q^p + Q^a + Q^s + Q_i^h - Q^v - Q_i^{trans} \quad = mc\Delta Temp_i$$

Variable Name	Variable Name	Unit
Setpoints (control)		
Heating energy: $Q_i^h = z_i P_{max} T$ $z_i \in \{0,1\}$ controls the period i in which, the power Pmax is applied.	Q_i^h	[Wh/period]
Outputs		
Thermal Energy difference in the house. The mass of walls is m = Area* Surface Density Area: Pwalls = 252 [m^2] Surface Density: mWalls = 125 [kg/m^2] Specific heat capacity of walls c = 840 [J/kg°C], $\Delta Temp_i$ temperature difference °C	$Q_{i+1}^{stored} - Q_i^{stored} = mc\Delta Temp_i$	[Wh/period]
Measurements/ state variables		
$\Delta \boldsymbol{T}emp$ is defined as the temperature difference between the **time varying** internal temperature and the external temperature. Thus, the time period index i	$\Delta \boldsymbol{T}emp_i$	[°C]
Energy lost due to the walls and windows conductivity. Depends on building materials as well as on the difference between outside and inside temperature $Q_i^{trans} = L^{trans} \ \Delta \boldsymbol{T}emp_i$ $L_{trans} = U \ P$ Where U [W/m^{2}K] is a measure of thermal resistance and P [m^2] is an area of a specific material.	Q_i^{trans}	[J/K/period]
Constraints		
Internal temperature range , e.g 18-22 °C	$[T_{\min}, T_{max}]$	°C
Heating power, e.g. 5000	$P_{\max}$	W
Parameters		
Energy generated by people residing in the house. Q^p= Area/personArea * usagePerDay * personEnergy PersonArea=45 m^2 UsagePerDay=24h PersonEnergy=90 W Changes in the number of people in 24h are not	Q^p	[Wh/period]

modelled.		
Energy generated by household appliances and lights. Q^a= consumption * area , e.g. consumption = 3W/m^2 area = 128m$^2_{Text}$	Q^a	[Wh/period]
Energy received from the sun is considered constant during a month. $Q^s = f(Date.month)$. In January for instance we obtain 139 Wh/period. Assumption: 40% glass surface, south orientation.	Q^s	[Wh/period]
Energy lost due to the ventilation. Depends on the difference between outside and inside temperature. (We assume this factor constant during a month). e.g. Q^v =11.25Wh/period	Q^v	[Wh/period]

Table 6 – Model parameters and variables

Example of calculation of Q^s , the energy increase because of the sun heat.

- Area windows: 30 m2
- SHGC solar heat generation factor : 0.389
- Solar radiation (60° latitude) , 90 degrees (vertical windows)
- 20 MJ/m2/day
- Q^s= 0.389*30* 20 *0.278/24 = 2.7 kWh

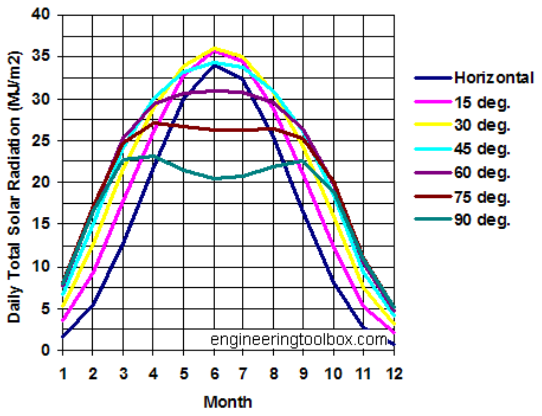

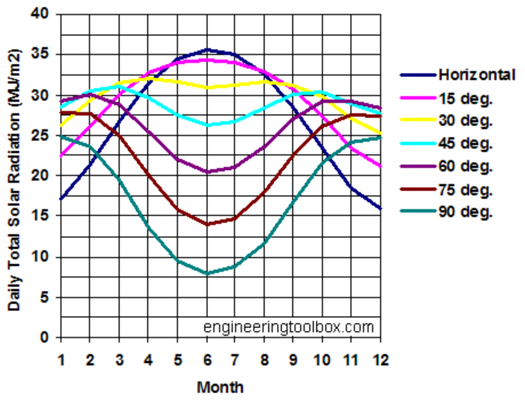

Figure : Sun radiation at 60°N latitude, Sun radiation at 30°N latitude

Infiltration heat loss Q^v [6]:

c_p = specific heat air (kJ/kg K) = 1.005
ro_{air} : density of air = 1.205 kg/m3
n = air_shifts/h = 0.4
V is the air volume

[6] http://www.engineeringtoolbox.com/heat-loss-buildings-d_113.html

$Q^v/(T_{in}-T_{out}) = c_p\ ro_{air}\ n\ V\ [kWh]$

Heat from Lighting Q^a

- 4 W/m2
- Area: 3134 m2

$Q^a = 4*3134 = 12{,}5\ kW$

Heat from persons Q^p

- m2 per person = 35 m2
- Usage 24 h
- Person energy : 90 W
  f_p = 3134/35 * 90 = 8,58 kWh

B APPENDIX : COMPONENTS DEFINED IN IRENE

Component	Description	Attribute1	Attribute2: consequence
High voltage line	Long range connection: national or international HV power supply	Physical damage: strong storm, floods, quake	
Electricity connection	Power line.		
Primary power substation	Prev. connector adaptor. MV power station including SCADA	Crucial: physical and cyber attack,	
Secondary power station	(microgrid connection) includes transformer to LV (0.4kV) and MG controller	Physical damage and cyber attack on controller and comm. connection	
Local power plant	Local (as node of the simulated grid) generation: coal, gas, oil, hydro. Includes SCADA.	If fails, contingency scheme activated.	
Renewable generation (PV, wind)	Local power plant as node in the simulated grid.		
Large Battery Storage	Node of the grid		low
Stadium	Large load		low critical if not in use or not planned as shelter
Basic House	Single house, 250sqm with PV, EV, air condition and battery.	De-aggregated data available	
Small office	512 sqm office	De-aggregated data (US): ICT , lights are critical loads.	Consequence: Bank: high
Supermarket		Light, ICT and refrigeration (50% of consumption) are critical loads.	
Midrise apartment block			

Assets that could be added to the CEMS control

Generic grid model	Configuration	demand type	Model Parameters	Additional rule

HVAC	yes	Flexible (model)	See thermal parameters	Policy rule: disable during outage
EV	yes	Flexible (model)	charging period, min., max. demand	Policy rule: disable during outage
Kitchen, enter-tainment	no	Interruptible profile		
Lighting (partial)	no	critical profile		
Comm.: wire/ cell, computer	No	In critical profile		
CEMS controller, AMI	no	In Critical profile		
Water, gasoline pump (TBD)				
Fridge (TBD)		Flexible, mod-el	Pmax, T_min, T_max	Policy rule
PV gen	yes	Flexible, mod-el	P_rated	Policy rule
Hotwater (TBD)				
ESS, Battery	yes	Flexible, mod-el	Charge_rate, Dis-charge_rate, capacity, SOC_init, efficiency	Policy rule

C Appendix : On the Concept of Resilience in Cyber-Physical Systems

The word “resilience” means literally *the capacity to recover quickly from* difficulties, or *the ability of a substance or object to spring back into shape* (Oxford Dictionary Online). The word is used with reference to materials recovering elastically after being compressed, and also in a variety of disciplines to designate properties related to being able to withstand shocks and deviations from the intended state and go back to a pre-existing, or a desirable or acceptable, state (Strigini 2012).

The word resilience has become popular in recent years especially in the area of information and communication technology (ICT) and policy related to ICT. The use of the term resilience indicates a broadening of perspective compared to traditional Information and Communication Technologies (ICT) system assessment notions such as reliability and availability (Strigini 2012).

This is a general trend, and resilience is a term used commonly in other fields than ICT. For instance, in the broad Engineering field, according to Wikipedia, it is distinguished between resilience in *material science*, in *engineering and construction*, and *networks*. Other possible contexts are organisational or ecosystem resilience, or psychological resilience (the ability to deal with stress) (AMBER 2009); also, the term resilience is largely present when discussing on protection of critical infrastructure (DHS 2009). In such uses, the term resilience usually refers to the robustness in the presence of change, most commonly disasters, or to the ability of a network to deliver acceptable service in the presence of faults (Strigini 2012), (AMBER 2009). It should be noted that similarly, (Avizienis et al. 2004) equate resilience with fault tolerance.

Connected to the above discussion, *resilience assessment* is interpreted to mean assessment of systems in evolving environments and conditions and in the presence of faults or failures of any kind. How to measure or benchmark resilience is a difficult open problem, that may have different answers and approaches depending on the target system. One of the big challenges faced in resilience assessment is the lack of standardized assessment of ICT systems and components. Benchmarks are very common in performance, but struggle to gain a foothold in resilience assessment (AMBER 2009). As resilience is a broad concept encompassing multiple attributes, there are multiple possible measures. From (Strigini 2012), we summarize three possible broad *categories of measures* related to resilience assessment:

- *measures of dependability in the presence of disturbances*, which may be estimated empirically in operation or in a laboratory, or through probabilistic models (as functions of measures at component level);

-measures of the *amount of disturbances that a system can tolerate*, typically obtained from analysing a system’s design;

- measures of *probability of correct service given that a disturbance occurred* (“coverage factors”).

Focusing on Smart Grids and Smart Cities, the term resilience is also often use. For example, in (Neirotti 2014) resilience of smart cities is considered, and closely matched to vulnerabilities, anomalies and security issues. Although we acknowledge that resilience may be also intended in a broader sense, it is important to remark that (Neirotti 2014) states that “**policy-**

makers and city planners should therefore **take** vulnerability, **resilience**, financial sustainability and social inclusion into consideration in their approaches to build cleverer cities": this position is well-aligned to the IRENE project and objectives. Instead (Albasrawi 2014) consider resilience in the Smart Grid context as *the ability of a system to bounce back from a failure* (Henry 2012), and defines a related metric, based on the provided system's functionality and performance. (Fang 2012) is aiming to improve resilience to disruption on Power Grid, while (Gungor 2011) and (Pin-Yu 2012) discuss on network resilience in Smart Grids.

Very recently, according to (Bollinger, 2015; Cano-Andrade, von Spakovsky, Fuentes, Lo Prete, Hobbs, & Mili, 2012), the resilience is defined as *the ability of a power system to recover to a new original state from an unanticipated event that causes a failure to the system*. The authors (Bollinger, 2015; Cano-Andrade, et al., 2012; Khodaei, 2014b) further extended the resilience concept by stating that resilience is *the ability of a power system to withstand/remain in a state during a failure in an efficient manner, and to quickly restore to the normal operating state*. We can observe that this last definition, presented for a context and purpose very fitting for IRENE, is fully compliant with the above discussion on the concept of resilience. Consequently, we adopt this definition for the current deliverable.

In order to assess resilience, the same work (Bollinger, 2015) defines a performance metric indicator. Such metric presents the extents in which the amount of energy demand within consumers are met when there is a disturbance in the grid (Bollinger, 2015). The performance metric to calculate the resiliency is based on the fraction of demand served (Bollinger, 2015; Cano-Andrade, von Spakovsky, Fuentes, Lo Prete, Hobbs, & Mili, 2012).

As in line with (Bollinger, 2015; Cano-Andrade, von Spakovsky, Fuentes, Lo Prete, Hobbs, & Mili, 2012), the resilience in this case is therefore the mean fraction of demand served ($P_{D,t}^{c'}$) across the outage events divided by the overall demand ($P_{D,t}^{c}$) in the contingency state:

$$\alpha_{\text{Resiliency}} = \sum_{t=1}^{NT} \frac{P_{D,t}^{c'}}{P_{D,t}^{c}}. \qquad (c = 1, \ldots, NT) \qquad (31)$$

(AMBER 2009) AMBER Consortium. D2.2—state of the art (final version). Technical report, AMBERConsortium, July 2009]

(Strigini 2012) Strigini, Lorenzo. "Fault tolerance and resilience: meanings, measures and assessment." Resilience Assessment and Evaluation of Computing Systems. Springer Berlin Heidelberg, 2012. 3-24.

(Avizienis et al. 2004) A. Avizienis, J.-C. Laprie, B. Randell, C.E. Landwehr, Basic concepts and taxonomy of dependable and secure computing. IEEE Trans. Depend. Secure Comput. 1(1), 11–33 (2004)

(DHS 2009) Department of Homeland Security - National Infrastructure Advisory Council, Critical infrastructure resilience: final report and recommendations, 2009, https://www.dhs.gov/xlibrary/assets/niac/niac_critical_infrastructure_resilience.pdf.

(Neirotti 2014) Neirotti, Paolo, et al. "Current trends in Smart City initiatives: Some stylised facts." Cities 38 (2014): 25-36.

(Albasrawi 2014) Albasrawi, Murtadha N., et al. "Analysis of reliability and resilience for smart grids." Computer Software and Applications Conference (COMPSAC), 2014 IEEE 38th Annual. IEEE, 2014.

(Henry 2012) D. Henry and J. E. Ramirez-Marquez, “Generic metrics and quantitative approaches for system resilience as a function of time,” Reliability Engineering & System Safety, vol. 99, pp. 114 – 122, 2012.

(Gungor 2011) Gungor, Vehbi C., et al. "Smart grid technologies: communication technologies and standards." IEEE transactions on Industrial informatics 7.4 (2011): 529-539.

(Fang 2012) Fang, Xi, et al. "Smart grid—The new and improved power grid: A survey." IEEE communications surveys & tutorials 14.4 (2012): 944-980.

(Pin-Yu 2012) Chen, Pin-Yu, Shin-Ming Cheng, and Kwang-Cheng Chen. "Smart attacks in smart grid communication networks." IEEE Communications Magazine 50.8 (2012): 24-29.